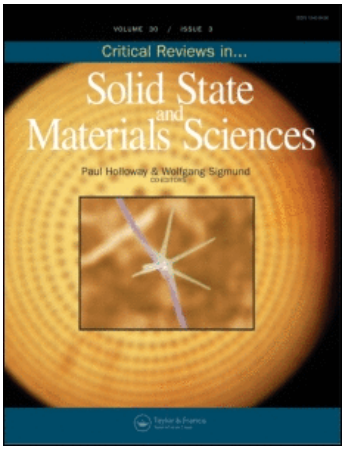

Critical Reviews in Solid State and Materials Sciences
Publication details, including instructions for authors and subscription information:
http://www.informaworld.com/smpp/title~content=t713610945

Reciprocal space mapping

Paul F. Fewster [a]
[a] Philips Research Laboratories, Redhill, U.K.

To cite this Article Fewster, Paul F.(1997) 'Reciprocal space mapping', Critical Reviews in Solid State and Materials Sciences, 22: 2, 69 — 110
To link to this Article: DOI: 10.1080/10408439708241259
URL: http://dx.doi.org/10.1080/10408439708241259

Critical Reviews in Solid State and Materials Sciences, 22(2):69–110 (1997)

Reciprocal Space Mapping

Paul F. Fewster
Philips Research Laboratories, Cross Oak Lane, Redhill, RH1 5HA, U.K.

ABSTRACT: This review covers the recent advances in reciprocal space mapping. The experimental techniques as well as the theoretical and conceptual developments are discussed. The advantages of reciprocal space mapping over the conventional single scan X-ray scattering methods become clear from the examples presented. Extracting the additional information from mapping in reciprocal space maps has led to a deeper understanding of materials. Imperfect materials benefit enormously from these methods. Near perfect materials also indicate weak diffuse scattering that can now be interpreted in terms of defects, etc., whereas with single scans the influence is difficult to observe and separate from other features. Reciprocal space maps can be collected with both high and low angular resolution diffractometers, depending on the application, although a combination of resolutions may be necessary. It is also growing in importance in the analysis of materials using specular reflectometry. High-resolution reciprocal space mapping is not restricted to good crystalline quality. Examples of reciprocal space mapping are given for semiconductors, metals, ceramics and biological samples. For semiconductor materials, reciprocal space mapping has now become almost routine in the study of lattice relaxation in thin layers and in the assessment of the "quality" of materials. Combinations of mapping with topography and precision lattice parameter determination are also discussed. The latter part of this review discusses the advantages of three-dimensional reciprocal space mapping, which takes the analysis further. With this method the full three-dimensional shapes in reciprocal space can be studied.

KEY WORDS: reciprocal space mapping, X-ray diffraction techniques, X-ray scattering methods.

I. INTRODUCTION

Reciprocal space mapping is a general term used to describe the recent developments in the methods of data collection using X-ray diffraction techniques. The principle is to extract as much information from the X-ray diffraction pattern as possible by restricting the diffraction space probe and surveying reciprocal space in great detail. This greater detail can lead to information on the microstructure and deviations from perfection that can often dominate the physical properties of materials. This is similar to reproducing digitized film methods but with a far smaller probe and much higher dynamic range. The emphasis of this review is on the application of diffractometers with exceedingly high angular resolutions for very precise work and low angular resolutions for enhanced intensities of poorly diffracting materials. It will become clear though that in general a combination of these two approaches is close to the ideal. The full range of analysis methods for materials by X-ray diffraction techniques is very extensive, and the present role of reciprocal space mapping can be seen in context from a recent review (Fewster, 1996a).

In general, the resolution should be chosen to suit the problem, for example, a sam-

1040-8436/97/$.50

ple that creates broad reciprocal space features may not require high-resolution reciprocal space mapping. This is because the smearing effects of the diffractometer may be significantly less than the reciprocal lattice features. The data collection can be unnecessarily long and low-resolution reciprocal space mapping may well be more appropriate, at least initially. It is of course important to be aware of the shape of the reciprocal lattice features, because if they are highly anisotropic a scan through a narrow section may require high resolution as in the case of unstrained highly mosaic crystals. Simply, the resolution depends on the information required and the more uncertainty there is regarding the sample, and therefore the assumptions concerning its structure, the higher the resolution should be. To extract structural information associated with the profile shape than generally high resolution should be considered first, whereas if only the peak positions are of interest then perhaps low-resolution reciprocal space mapping will suffice. Clearly, there are no definitive rules for an unknown sample, and the possibility of using both high- and low-resolution reciprocal space mapping is an advantage. Examples of both high- and low-resolution applications are presented in this review.

Any sample that we wish to analyze is three-dimensional and therefore the three-dimensional shape is the ultimate goal. Single profile and two-dimensional reciprocal space mapping require making assumptions about the sample because they are, respectively, projections of a plane or a line in reciprocal space. The development of three-dimensional reciprocal space mapping (this restricts the projection in three dimensions) is discussed with examples of how much more information is contained in this type of data. The method has been applied to protein crystals, polycrystalline samples, and imperfect semiconductors, etc.

II. LOW-RESOLUTION RECIPROCAL SPACE MAPPING

A. The Principle and Method

Low-resolution reciprocal space mapping is much more akin to conventional film techniques, except that the data are collected digitally and generally with a single detector. The simplicity of the geometry of the low-resolution slit-based instrument for reciprocal space mapping is given in Figure 1. The data are collected with radial scans (rotating ω and $2\omega'$ together such that $\Delta\omega = \Delta\omega'$) each being offset by an angle $\delta\omega$ from the previous). For low-resolution reciprocal space mapping, the beam is not conditioned by crystals but by slits. A slit-based system defines the beam spatially to give an angular precision. This results in instrumental broadening that can dominate the diffracted beam profile unless the sample contributes significantly. The broadening arises from the spectral distribution of the source and the distribution of incident angles across the sampled region. The smearing or instrument probe function for such a system is given by Fewster and Andrew (1996a), who have determined this shape experimentally. Slit-based diffractometers are less useful for obtaining details of profile shape because of the influence of the sample type, degree of orientation texture, etc. Similarly, the peak positions are less reliable because sample centering, or effective centering due to absorption, on the diffractometer axes displaces the apparent scattering direction.

Low-resolution reciprocal space mapping has the advantage of increased intensity for probing weakly diffracting samples, but has the significant disadvantage of large instrumental smearing effects. In general, this low resolution is a consequence of using slits, especially at the detector end, hence the scattered beam direction is defined by its position in space and not by the scatter-

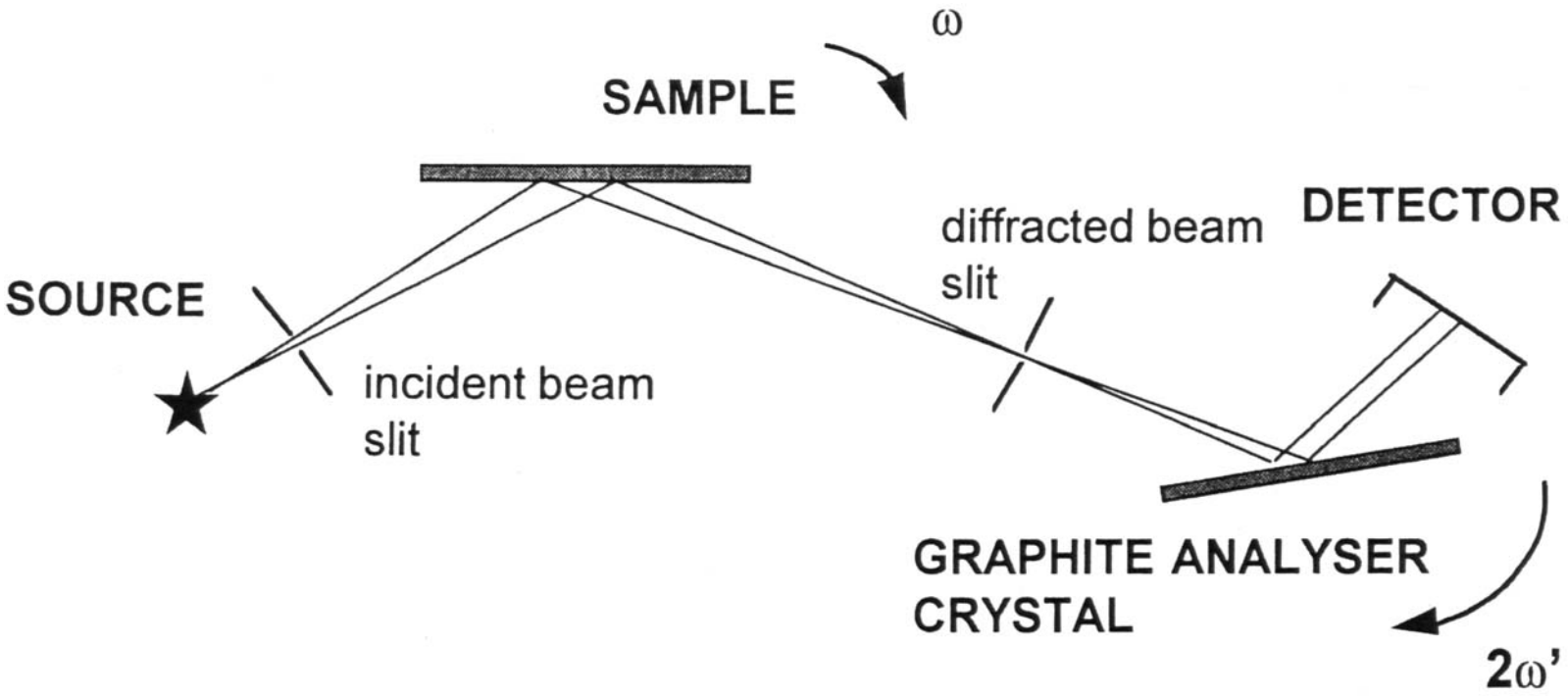

FIGURE 1. A diffractometer for obtaining low-angular resolution reciprocal space maps. The incident X-rays and scattered X-rays are defined by slits. The graphite analyzer crystal is mosaic and can act as a course energy filter to reduce unwanted wavelengths and fluorescent background.

ing angle directly. Van der Sluis (1993) has used a combination of a high-resolution monochromator and a slit in front of the detector to study samples that scatter weakly but still require reasonable resolution. Because of the spatially large beam from the monochromator, the angular resolution of the scattered beam is poor. However, if the projected view of the sample as seen by the detector is reduced and a matching slit is inserted in front of the detector, the angular resolution can be improved. This approach is suitable for applications with scattering angles, $2\omega'$, close to the incident glancing angle, ω, for example, mapping the diffraction from inclined crystal planes. Often, the positions of scatter maxima is sufficient for many applications and this form of analysis with slit collimation throughout can prove very useful (Fewster and Andrew, 1993a). Thompson, Collins, Doyle and Knapp (1991) have combined a double-crystal diffractometer with a position-sensitive detector to collect reciprocal space maps rapidly. Position-sensitive detectors do have far lower saturation levels compared with conventional detectors, which can be troublesome for reliable intensity measurements. This method is applicable to studies of reflections that match that of the collimating crystal, and therefore realignment of the double crystal diffractometer is necessary to avoid very different instrument smearing functions for studies at other scattering angles.

Three-dimensional reciprocal space maps can also be performed with slit-based systems (Fewster and Andrew, 1996a), although the instrumental smearing and complications of zero errors limit the applications of the method. However, it still improves the basic two-dimensional map data. The other essential difference between the high-resolution (based on crystal optics) and low-resolution (based on slit confinement of the beam) probes is that with the former the intensities can be placed on an absolute scale, the angles can be defined on an absolute scale (Fewster and Andrew, 1995b), and the probe shape is well defined and thus capable of achieving detailed analysis of the diffraction profile shape.

Of course, low-resolution reciprocal space mapping is not restricted to $\omega/2\omega'$ against ω as this is only one projection, which happens to contain considerable quantities of information. A standard pole figure for determining the orientation distribution is a projection of the intensity distribution on the sample surface for a finite integration depth defined by $\Delta 2\omega'$. Similarly, the multiple diffraction studies of Rossmanith and Bengel (1995) are reciprocal space maps of $\omega/2\omega'$ vs. the azimuthal, or crystal rotation about the surface normal, angle ϕ. However, to contain the length of this article, I will not extend the review to include analyses of all the possible projections.

B. Applications of Low-Resolution Reciprocal Space Mapping

1. Twinning

Reciprocal space mapping obviously becomes most significant when no other approaches can easily yield the desired information. One such case arose with the attempts to obtain the twin proportions of the high-temperature superconductor $YBa_2Cu_3O_{7-\delta}$ sputtered on $SrTiO_3$. The in-plane lattice parameters of the orthorhombic form of $YBa_2Cu_3O_{7-\delta}$ are very similar to that of $SrTiO_3$ and therefore has a finite probability of existing in two rotations 90° apart. No simple single scan could be performed that would give the scatter contributions from the two "twin" components. A reciprocal space map close to the 038 reflection of one twin component will also show the 308 reflection from the other (Fewster and Andrew, 1993a). Mea-

surement of the integrated intensity from these two reflections have been related to the calculated intensities and the proportion of the two twin components obtained. Because these reflections were so weak, the peak intensity was inadequate to evaluate a reliable estimate of the scatter proportion.

2. Relaxation Studies

When the features of interest have broadening effects that are significantly greater than the instrumental smearing effects, then valuable information can be obtained quite readily. Hart and Fewster (1993) have investigated the influence of growth of very thin (60 and 400 Å) InAs semiconductor layers on the (110) surface of GaAs. The intention here was to observe whether the nature of the dislocations could be controlled by restricting the allowable Burgers vectors to certain directions at the interface. Only the {111} slip planes are inclined to the surface in the [−110] surface direction and not the [001] surface direction for a (110) orientated surface plane. Hence, only strain relief along the [001] direction is possible and not along the [−110] direction from 60° dislocations, whereas 90° Lomer dislocations could relieve the stresses in the orthogonal direction (Zhang, Pashley, Hart, Neave, Fawcett, and Joyce, 1993). The possibilities of tilting are also only likely to occur about the [−110] axial direction if this is a consequence of the inclined Burgers vectors. The scattering is clearly very weak from a highly distorted relaxed and therefore mosaic 60 Å layer, but the necessary features of interests are clearly seen with the low resolution reciprocal space mapping geometry.

A combination of the 220, 620, and 331 reflections were used to extract the lattice parameters normal and parallel to the surface plane. The results showed that the unit cell had relaxed anisotropically in the thin layer with negligible tilting, but for the 400 Å layer the relaxation had become more symmetrical, but the layer to substrate tilting was close to 1.0°. To obtain more information, the samples were analyzed using multiple crystal topography (Fewster, 1991b) by imaging the contrast from the diffuse scattering close to the substrate reflection. For (001) orientated surfaces an orthogonal array of dislocations would be observed, but in these examples only short segments of dislocations clusters could be observed. The number ratio of the dislocation clusters in the two orthogonal directions correlated with the ratio of 60° to Lomer dislocation densities found in TEM. The change in anisotropic strain relaxation is explained by the very low "critical layer" thickness of less than one monolayer. So that in the early stages of growth edge dislocations can form before uniform coverage of the InAs exists. The 60° dislocations form because of the high stress levels giving significant relaxation in orthogonal directions. As the layer thickness increases only 60° dislocations can be generated, leading to an anisotropic relaxation, and because the contributing {111} slip planes are not equivalent, this could well result in the net macroscopic tilting observed. The short segments of the dislocation clusters were explained by the interaction of the two different types of dislocations.

The use of low-resolution reciprocal space mapping in this case is clearly adequate to a point, because the scattered intensity is weak and the peak shapes have become diffuse to a greater extent than the instrument smearing effects. However, the high-resolution technique of topography had to be employed to confirm aspects of the analysis.

Thompson, Collins, Doyle, and Knapp (1991) have characterized silicon on insulators using a double crystal diffractometer and position-sensitive detector that proved very effective and yielded mosaic spread

values of ~0.2° and strains of ~0.08%. Picraux, Doyle, and Tsao (1991) have also used this instrument for studying InGaAs/GaAs strained layer superlattices where they could clearly observe macroscopic tilting between the substrate and the layer structure. Olsen, Hu, Lee, Fritz, Howard, Hammons, and Tsao (1996) have used the same approach to study linearly graded buffer layers of InAlAs on GaAs. Olsen et al. determined the unit cell parameters from the reciprocal space maps and found the relaxation to be less than the equilibrium value for this structure, but, interestingly, could not induce further relaxation by annealing, abrading the surface (to introduce dislocations), and annealing. This obviously has consequences if control of the unit cell dimensions is required for subsequent growth. This relatively rapid approach to obtaining reciprocal space maps therefore can be used very successfully for the analysis of the main diffraction features.

Van der Sluis (1993) used a four-crystal monochromator to collimate and the incident beam divergence and chose an appropriate reflection that gave a very low angle of exit from the sample; this combined with the detector slit to match the width of the scattered beam for a perfect sample made it possible to effectively improve the angular resolution. A SiGe multilayer was studied in this way and was found to be almost completely relaxed (Figure 2). There was sufficient information in this map for him to determine the state of strain in each layer.

Metallic multilayers pose interesting problems for X-ray diffraction analysis, especially when they are partially relaxed and the compositions are uncertain. Birch, Sundgren and Fewster (1995) have analyzed a Mo/V (001) superlattice magnetron sputtered onto a MgO (001) substrate. The unknown parameters are the lattice parameters normal and parallel to the surface for each component and the individual layer thicknesses. These parameters are important because the introduction of H into the structure can also dilate the vanadium layers (Birch, Hjörvarsson, and Sundgren, 1994). The theoretical reasoning given by Birch, Sundgren, and Fewster was to reduce the number of parameters by correlating the results of reciprocal space mapping and reflectometry by just assuming the Poisson ratios of the constituents. Similarly, if the lattice parameters were known the Poisson ratio's could have been determined. The scattering close to 000, that is, the specular reflection, is just sensitive to chemical modulations, whereas at higher scattering angles strain components are also present. As shown in Figure 3, combining information from inclined planes as well as those parallel to the surface will give components of the lattice parameter that are parallel and perpendicular to the surface, respectively. The reflectometry profile yielded the period and individual thicknesses by simulation. The scattering around the Bragg peaks gave the average perpendicular and parallel lattice parameters for the superlattice, and these are related to the actual interplanar spacing via a so-called composition fraction x_A such that:

$$\bar{d}_\perp = x_A d_{\perp A} + (1 - x_A) d_{\perp B}$$

and similarly for the interplanar spacings d parallel to the surface. The composition fraction is determined as

$$x_A = \frac{\bar{d}_\parallel - \frac{\bar{d}_\perp}{\Lambda}\left(\frac{d^0_{\parallel A} D_A}{d^0_{\perp A}\beta_A} + \frac{d^0_{\parallel B} D_B}{d^0_{\perp B}\beta_B}\right) - d^0_{\parallel B}\left(1 - \frac{1}{\beta_B}\right)}{d^0_{\parallel A}\left(1 - \frac{1}{\beta_A}\right) - d^0_{\parallel B}\left(1 - \frac{1}{\beta_B}\right)}$$

where d^0, D and Λ are the unstrained interplanar spacings, the layer thicknesses, and superlattice period, respectively. The value

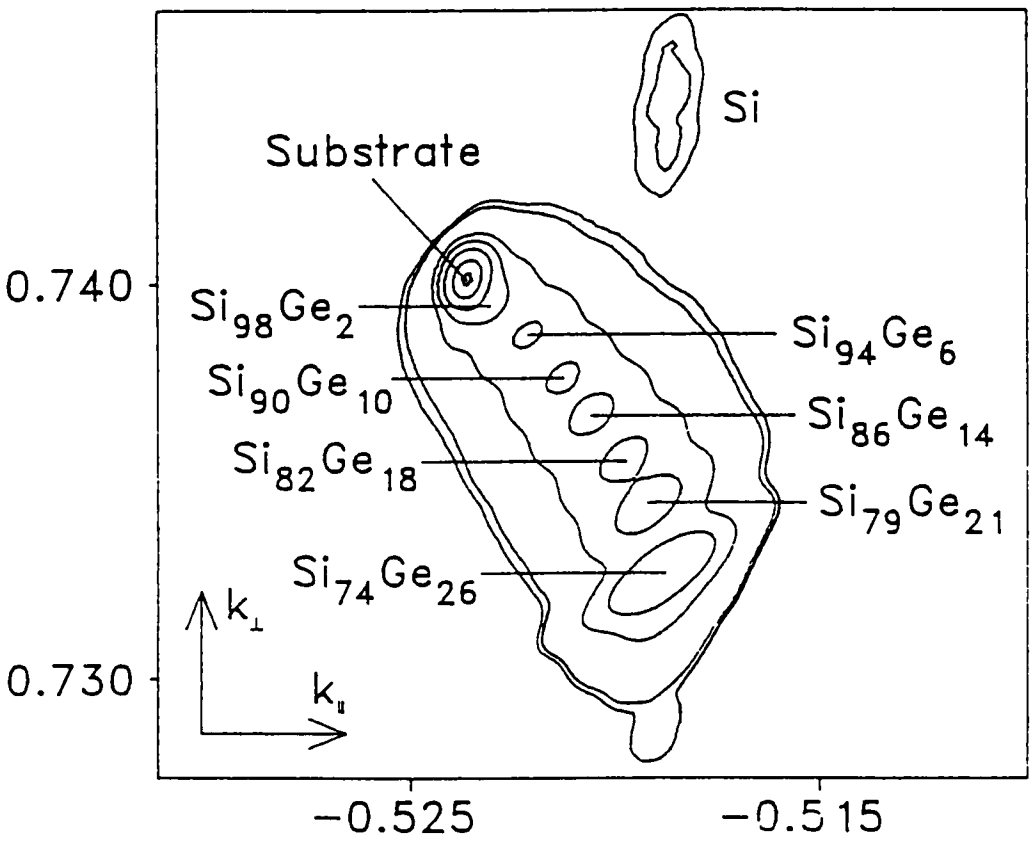

FIGURE 2. A reciprocal space map close to the 224 reflection from a multilayer SiGe structure showing the almost total relaxation of layers 1–6, whereas layer 7 is matched laterally to 6 and likewise the Si layer 8 and SiGe layer 9. The data were collected with a combination of monochromator and slit. (Courtesy of P van der Sluis.)

β_i is the ratio of elastic constants for layer A or B given by:

$$\beta_i = \frac{2\nu_i}{\nu_i - 1}$$

Hence, all parameters in determining x_A are known, and individual lattice parameters of the layers can be determined.

Reciprocal space mapping becomes most important for obtaining accurate values of $d_{\parallel}$. Choosing appropriate reflections for obtaining these parameters was very limited for this Mo/V superlattice because of the very small lattice parameters, and therefore the large regions of reciprocal space had to be investigated. In these particular samples, one third of the coherency strain was relieved. The final values of all the parameters that were determined were then included in a simulation of the measured 002 reflection (radial scan), and the agreement was very close based on kinematical scattering theory. This indicated the reliability of the method.

Of course, to obtain details of the long-range order as a function of depth, then a more precise reciprocal space probe is needed and this is demonstrated in Fewster and Andrew (1993a). It was clear that the complications of an extended probe are not sig-

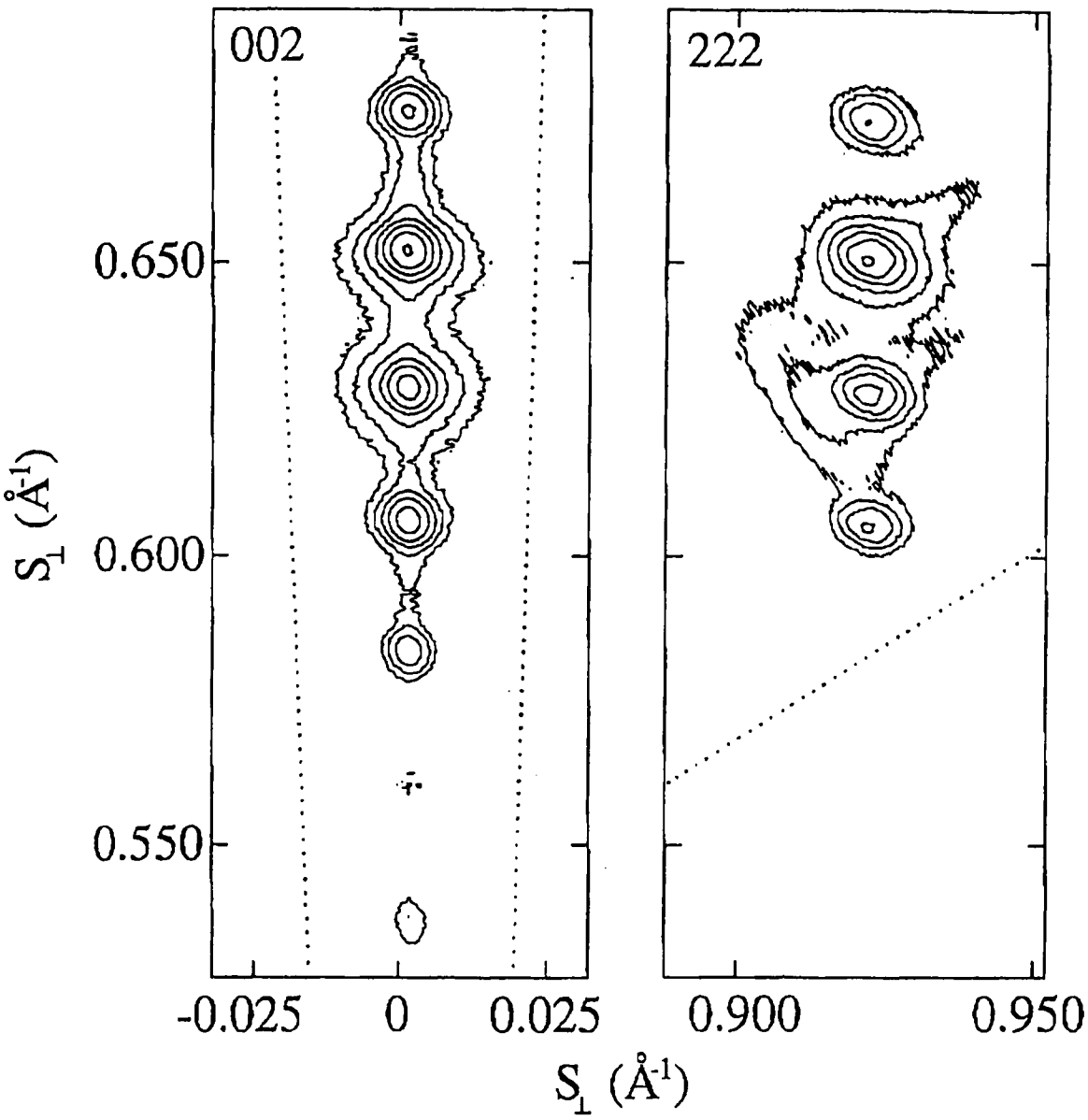

FIGURE 3. Two reciprocal space maps (close to the 002 and 222 reflections) of a Mo/V multilayer. The angular spread of the mosaic blocks was found to be less than 0.26° and the average lattice parameters could be determined. The diffractometer used was based on a divergence slit and a parallel plate collimator in the diffracted beam. (From J Birch et al.)

nificantly broadened and therefore are not sensitive to disrupted interfaces. This demonstrated the crucial difference between the high- and low-resolution methods in that the latter cannot be relied on to obtain true profile widths because of the extended reciprocal space probe. In this particular case, the measured radial scan width in high resolution was ~18" arc, whereas the dimension normal to this was approximately two-or-

ders of magnitude broader and therefore the scatter close to each reflection was very anisotropic. However, with low-resolution diffractometry the reciprocal space map indicated that the scattered intensity had a circular distribution, and therefore this smearing effect dominated the shape in reciprocal space.

3. Phase Identification

In the area of phase identification, reciprocal space mapping can also have significant impact. The use of collecting the complete accessible region of reciprocal space and integrating along ω the crystal rotation direction can recover reflections missing due to the presence of orientation texture (Fewster and Andrew, 1996a). Of course, the intensity values are not necessarily reliable, but the presence of identifying peaks are more likely to be observed. In a more sensitive mode for detecting weakly diffracting small contributions, a limited area reciprocal space map can be used to great effect.

Coast-Smith, Kidd, and Fewster (1996) analyzed a sample that was a light but hard alloy multilayer that was of relatively poor structural quality based on Ti and Al. Ti and Al alloy in many different forms and the presence of the face-centered cubic phase of Ti was thought to be a consequence of analytical sample preparation. This phase was observed in transmission electron micrographs and diffraction but not observed by X-ray diffraction techniques (Schectman, van Heerden, and Josell, 1994). After repeated careful scans the dominating peaks of this phase could not be observed using conventional techniques; however, a limited area reciprocal space map in the region of the identifying peak revealed a faint line that is detectable when viewed in this way but not when a single scan or indeed a group of scans are presented as a single line profile (Figure 4). The reason for this is that only a few Ti crystallites in this sample could be observed when it was rocked through 20°. Therefore, a conventional single scan has a very low probability of picking out the diffraction from these very sharp profiles. Therefore, the Ti (fcc) phase exists in this sample grown as described by Coast-Smith (1997) and is not a consequence of sample preparation techniques for transmission electron microscopy. The quantity of phase in this material is exceedingly small and probably less than a few percent of the whole.

Clearly, the value of mapping reciprocal space in this low-resolution configuration is very significant if the principal interest is in the positions of the peaks or for studying textured samples as in the example above. However, considerable care must be taken in the interpretation of the peak shapes unless of course the effects of interest cause broadening in excess of the instrument-smearing effects, unless of course the instrument-smearing effects are precisely known.

III. RECIPROCAL SPACE MAPPING AT VERY LOW INCIDENCE ANGLES

A. The Principle and Method

This topic is covered here in a separate section despite being based on similar principles to those of low-resolution reciprocal space mapping because the theoretical treatment and instrumental developments are slightly different. The emphasis here is on conditions when the incident beam is close to the critical angle for total external reflection. Total external reflection arises because

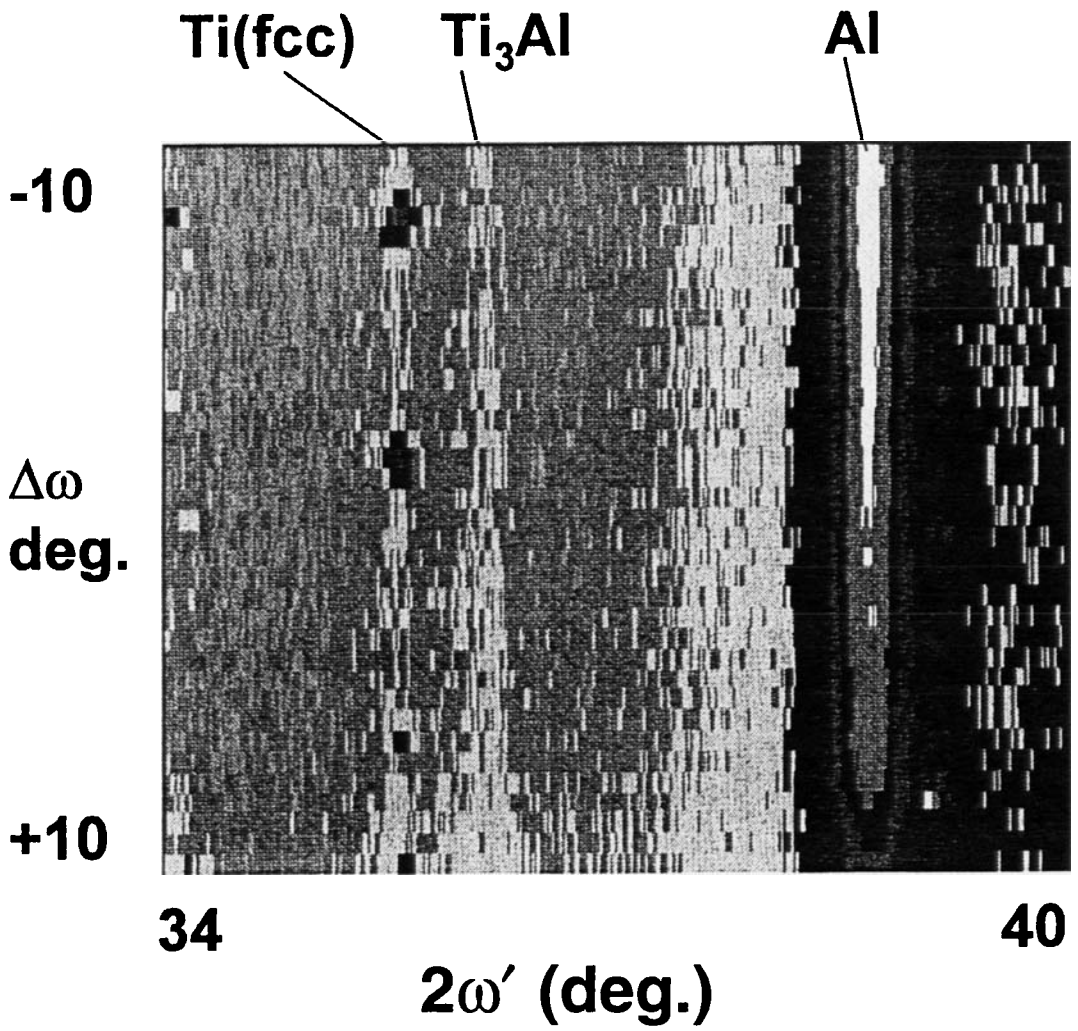

FIGURE 4. A low-angular-resolution reciprocal space map, from a polycrystalline metal sample, showing that very weak scattering can be observed in this way that could be unobservable using standard single scan methods. This approach relies on the abilities of the eye to observe fluctuations in two dimensions rather than relying on subtle peaks in one-dimensional noisy data.

of the refractive index for X-rays is less than one. The measurements are generally carried out in low-resolution mode as described above, although highly parallel synchrotron beams are used in some cases. For specular reflectometry and the analysis of its associated diffuse scattering, the theory can be much more straightforward than in the case of diffraction from higher scattering angles because the scatter is only sensitive to the X-ray density and not the atomic structure. However, on the other hand, mapping the intensity in reciprocal space in diffraction when both specular and diffracted beams are present can prove much more complex.

Because of the small deviation of the refractive index from unity, the critical grazing angle is typically a few tenths of a degree. This is easily achieved with crystal based collimation but the spatial extent of the beam usually requires large samples without a significant loss of intensity. Consequently, slit-based collimation in combination with a small X-ray source is typical (line focus with a 40-μm cross-section and 40-μm incident beam slit, with a laboratory-sealed source). The geometry can be as in Figure 1.

B. Applications of Reciprocal Space Mapping at Very Low Incident Angles

Interest in the use of reflectometry using low-resolution reciprocal space mapping has grown significantly in recent years because of the considerable diffuse scattering observed at these low angles. The diffuse scattering reveals information on interfacial roughening in the same way as that observed at higher scattering angles, although the effects can be much more pronounced. This can lead to complications in modeling the specularly scattered intensity because of the high background contribution.

1. Studying Interfacial Roughening

It has been known for some time that the interfacial roughness can be related to a lateral correlation length and evaluated assuming a fractal surface (Sinha, Sirota, Garoff, and Stanley, 1988). This lateral correlation length parameter can be determined using a single scan perpendicular to a radial scan and the resultant profile can be simulated. However, a reciprocal space map can reveal quite a complex distribution of diffuse scattering (Holý and Baumbach, 1994). Holý, Baumbach, and Bressière (1995) show that the measured maps can clearly indicate resonant diffuse scattering features that can be modeled using the scattering theory based on the distorted wave Born approximation. The sample they studied was an AlAs/GaAs superlattice, and this diffuse scatter model allowed them to show that the interfacial roughness was correlated from layer to layer. Similar analyses have been performed on oxide multilayers by de Boer, Leenears, and Wolf (1995), where again the "banana"-shaped resonant diffuse scattering features associated with the satellite peaks could be observed and modeled (Figure 5). The diffuse scattering in this region is complex and produces impressive reciprocal space maps. This is not only because of the resonant diffuse scattering but also because of the combinations that arise where the incident or exit beam approaches the critical angle and creates enhanced intensity, giving a complete cross-hatch of features.

In less uniform materials, the diffuse scattering can be quite homogeneous but is still interpretable as Stömmer, Grenzer, Fischer, and Pietsch (1995) have found in Langmuir-Blodgett multilayers of stearates.

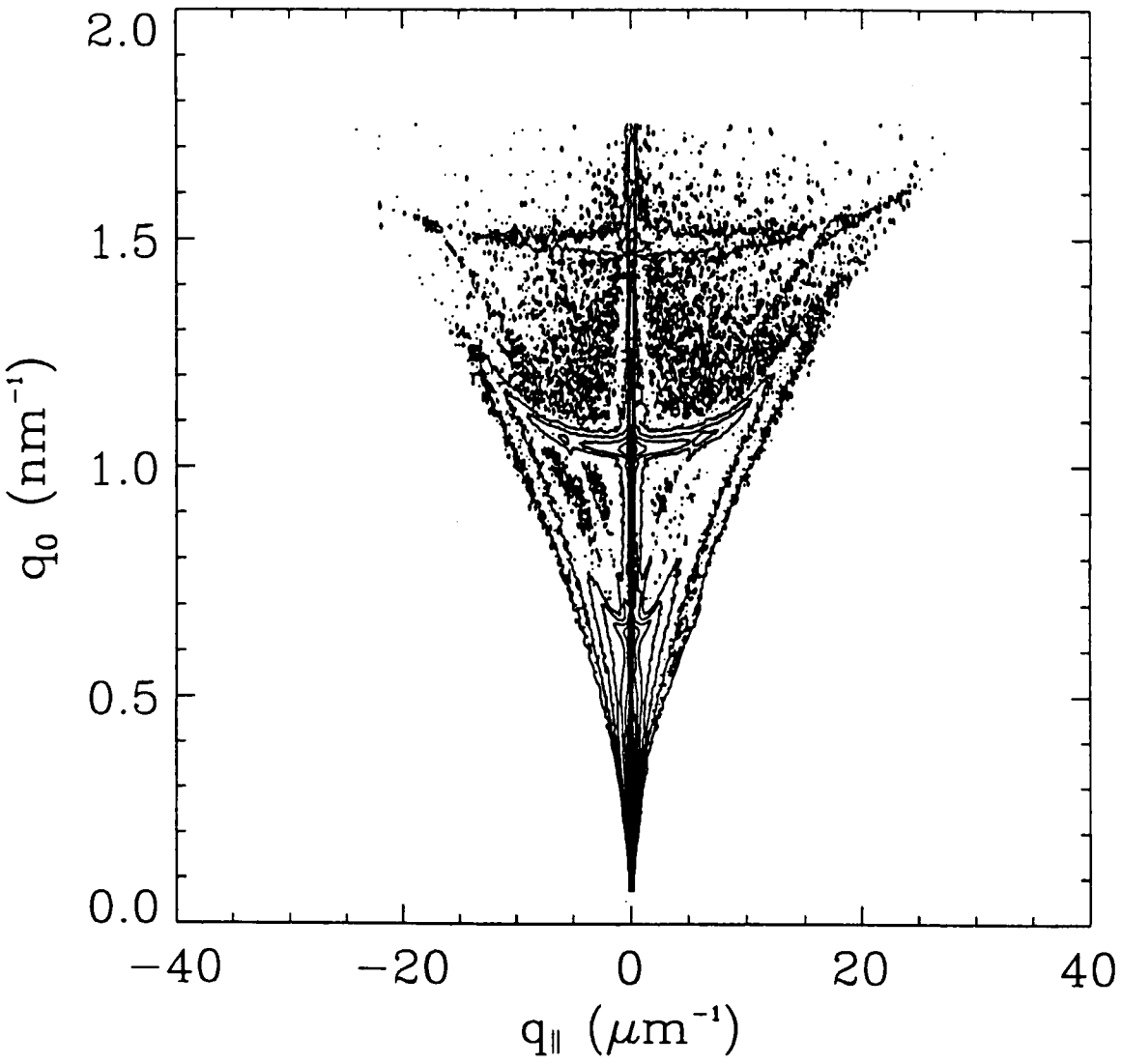

FIGURE 5. A low-resolution reciprocal space close to the origin of reciprocal space for a $MgO/MgFe_2O_4/Fe_3O_4$ periodic multilayer. The specularly reflected beam is at $q_{\|} = 0$ and the diffuse scattering "bananas" pass through the satellite reflections. The Yoneda wings and cross-hatched pattern are clearly visible in this map. (Courtesy of D K G de Boer.)

They could obtain information on the domain structure in these materials.

2. Diffuse Scattering Studies to Isolate Amorphous and Crystalline Components

Of course, grazing incidence diffraction will also have a specular component and vice versa, and therefore this should be considered when analyzing any scattering pattern, especially at very low incidence angles (Holý, 1996). Stepanov, Kondrashkina, Schmidbauer, Köhler, Pfeiffer, Jach, and Suvirov (1996) have treated this phenomenon using a combination of the dynamical diffraction theory and the distorted wave Born approximation and have shown that this leads to important subtleties in the dif-

fuse scattering. The diffuse scattering close to the specular wave is a consequence of fluctuations in the X-ray density, whereas the diffuse scattering close to the diffracted wave is sensitive to fluctuations in the crystal structure, making the latter that much more complex. For incidence angles below the critical angle the wave is purely specular if the sample is perfect, creating a simple cut-off in the diffracted intensity. However, if surface roughness is present then the diffuse scattering close to the diffracted wave extends above and below the critical condition but has a dip in magnitude at the Bragg condition. Stepanov et al. have been able to calculate the diffuse scattering close to the diffracted wave direction and show that this dip corresponds to Yoneda maxima that occurs in the diffuse scattering close to the specular condition. Likewise, the simulated reciprocal space maps (shown as diffraction space maps) of this diffuse scattering also exhibit resonant diffuse scattering features. They have applied this method to an AlAs/GaAs multilayer structure and do indeed see a difference in the diffuse scattering and suspect that this difference arises from surface oxidation that destroys the atomic ordering and weakens the diffuse scattering close to the diffracted wave.

3. Measurement of Layer Lattice Relaxation

Another way of studying structural details is to use non-coplanar diffraction procedures (Marra, Eisenberger, and Cho, 1979). In this geometry the incident beam subtends an angle very close to the critical angle so that the penetration depth can be controlled and when the sample is rotated about its surface normal diffraction can occur from planes normal to the surface plane. Jordan-Sweet, Mooney, Lutz, Feenstra, Chu, and LeGroues (1996) have used this approach to obtain the degree of relaxation in SiGe thin layers using reciprocal space maps. The data were collected on a synchrotron, and from this they were able to obtain details on the dislocation formation mechanism and accurate values of the composition and strain in these layers. The characteristic shapes of the scattered intensity in the reciprocal space maps revealed the relaxation mechanism. An approximately circular distribution corresponded to a roughening mechanism because of the significant lattice parameter variations, which could also be analyzed as a function of depth, whereas a cross-shaped pattern was indicative of a modified Frank-Read relaxation mechanism. Jordan-Sweet et al. could show qualitatively that the cross-shape could be described by introducing a distribution of diffraction vectors, including strain and rotation components associated with long-misfit segments known from early electron microscopy studies.

IV. HIGH-RESOLUTION RECIPROCAL SPACE MAPPING

A. The Principle and Method

As with any method the compromise between intensity and resolution is very important here. In general, the less that is known about the sample, the greater the requirement for understanding the performance of the diffraction space probe. The use of crystals to define the beam collimation generally reduces the available intensity compared with slit-based collimators, because the available divergence from the source is greatly reduced despite the fact that the beam cross-section can be much larger than that acceptable to slit-collimated diffractometers. The contributions to the diffraction space probe are different and consequently its shape can be very different. The known complications associated with

powder diffractometry are apparent with slit-based diffractometers, for example, sample height and sample size complications, etc. The nature of this reciprocal space probe has been discussed previously (Cowley, 1987; Iida and Kohra, 1979: Zaumseil and Winter, 1982; Fewster, 1989, 1991a, 1994, and 1996b) for high-resolution diffractometers (Fewster and Andrew, 1993a, 1996a), for slit-based systems and for a combination of high-resolution optics and slits (Itoh and Okamoto, 1988; van der Sluis, 1994).

Reciprocal space mapping has always been possible, but recent significant changes have come about from the versatility of the more recent diffractometers to match the increasing challenges in materials analysis. The ideal situation is to have a diffractometer that has a roughly constant diffraction space probe. Hence, the instrument does not require a complete rebuild to investigate different reflections from the same sample or for investigating different material systems. High-resolution reciprocal space mapping, for example, has been used very successfully in the study of semiconductor heterostructures. Perhaps the most widespread use has been in the study of layer relaxation when reciprocal space maps of several reflections have been combined to measure the residual distortions in the lattice repeat. The near constant reciprocal space probe permits the investigator to measure a range of reflections with the minimum of instrumental aberrations.

The reciprocal space probe of a triple crystal diffractometer is defined by the diffraction profiles of the first and third crystal (the second being the sample) and the wavelength dispersion through the whole instrument. The conventional double and triple crystal diffractometers are arranged such that the scattering angles of all the crystals, including that of the sample limit the wavelength dispersion, although the wavelength bandpass is large. However, because the wavelength bandpass is large any deviation from this "nondispersive" condition will create significant broadening of the reciprocal space probe.

The variable reciprocal space probe was a serious limitation of the conventional triple crystal diffractometer for high resolution reciprocal space mapping over large areas of reciprocal space. The diffraction space probe is also rather complex in shape because of the oblique interaction of the first and third crystal profiles. This can limit the resolution for precision investigations close to strong reflections without very careful convolution or deconvolution methods. Iida and Kohra (1979) used a triple crystal diffractometer with a channel cut collimating crystal and single reflection analyzer. This allowed them to explore reciprocal space close to the reflection of Si that matched the collimating and analyzer crystals. The artifacts (analyzer streak) was very significant and created complications in the reciprocal space map. Away from this special condition, the wavelength dispersion increases the complexity and worsens the resolution. However, Zaumseil and Winter (1982) investigated the improvements in the instrument probe by adding in extra reflections in the analyzer as well as the collimating crystal. These additional reflections reduced the extended diffraction profiles, thus decreasing the diffraction space probe without reducing the intensity (Bonse and Hart, 1965). However, the basic problem of a rapidly varying instrument function still existed. However, for high-angular-resolution studies of specific samples whose reflections match those of the monochromator and analyzer, the conventional triple crystal diffractometry is a significant improvement on the double crystal diffractometer. This is because the strain and mosaic components can be analyzed independently with the former.

The problem of the rapidly varying reciprocal space probe and maintaining the

small reciprocal space probe was overcome by reducing the wavelength bandpass by combining a four-reflection two-crystal monochromator with a multiple reflection analyzer (Fewster, 1989) (Figure 6). The wavelength-broadening effects over large areas of reciprocal space were greatly reduced and the artifacts from the extended diffractometer instrument profiles minimized. The intensity was still sufficient to achieve seven orders of magnitude dynamic range. Having the X-rays conditioned by crystals gives rise to an angularly narrow incident beam on the sample and an angularly defined acceptance of the scattered beam direction. The versatility of the high-resolution diffractometer has led to significant improvements, for example, by being able to place the reciprocal space maps on an absolute scale and the possibilities in combining these techniques with topography. These extensions are discussed next, because they both give valuable tools in aiding interpretation of reciprocal space maps.

B. Topography with High-Resolution Reciprocal Space Mapping

The angular resolution of a slit-based diffractometer is defined spatially and therefore because the angular variation changes from one area of the sample to the other. Consequently, for different regions of the sample to experience an equivalent incident angle, the sample has to be "rocked" about the ω axis. The major complication of the probe being defined spatially rather than angularly is that of interpreting the diffraction from an inhomogeneous sample. The high-resolution probe, on the other hand, is essentially utilizing a parallel beam whose divergence is defined by the intrinsic diffraction profile of the monochromator crystals, but this angular divergence has a negligible contribution to the beam dimensions and therefore all areas across the sampled volume experience the same incident beam conditions. Inhomogeneity in the sample will create an intensity variation in the scattered X-rays across the width and height of the diffracted beam from the sample being studied. Because all parts of the sample experience the same incident beam direction and intensity, any variation in contrast in the scattered beam can be observed on an X-ray-sensitive emulsion. X-ray sensitive film can be placed either in the diffracted beam directly from the sample Fewster (1991a) or after the analyzing crystal to pinpoint a region in reciprocal space Fewster (1991b).

The difference in resolution within the diffractometer plane and axial plane has also implications on the spatial resolution that is possible in topography. First, the axial divergence blurs out features, depending on how far the recording film is from the sample relative to the distance of the sample to the source. Clearly, to maintain intensity the beam paths are limited, and therefore the source is not necessarily optimized for topography. For the best spatial resolution in topographic images the film should be placed as close to the sample as possible. However, for high reciprocal space resolution the film has to be placed after the analyzer crystal, and consequently the spatial resolution is degraded. The spatial resolution normal to the plane of the diffractometer is typically 15 and 150 μm for positions 1 and 2 (Figure 6). The resolution in the diffractometer plane is largely controlled by the grain size of the developed emulsion, which is less than 1 micron for the best film, for film placed in position 1 of Figure 6. When the film is placed after the analyzer crystal, there is an additional smearing effect due to the finite penetration of the beam into the analyzing crystal. For the 220 reflection from Ge with CuKα (a commonly used combination), the resolution amounts to about 3 μm at most.

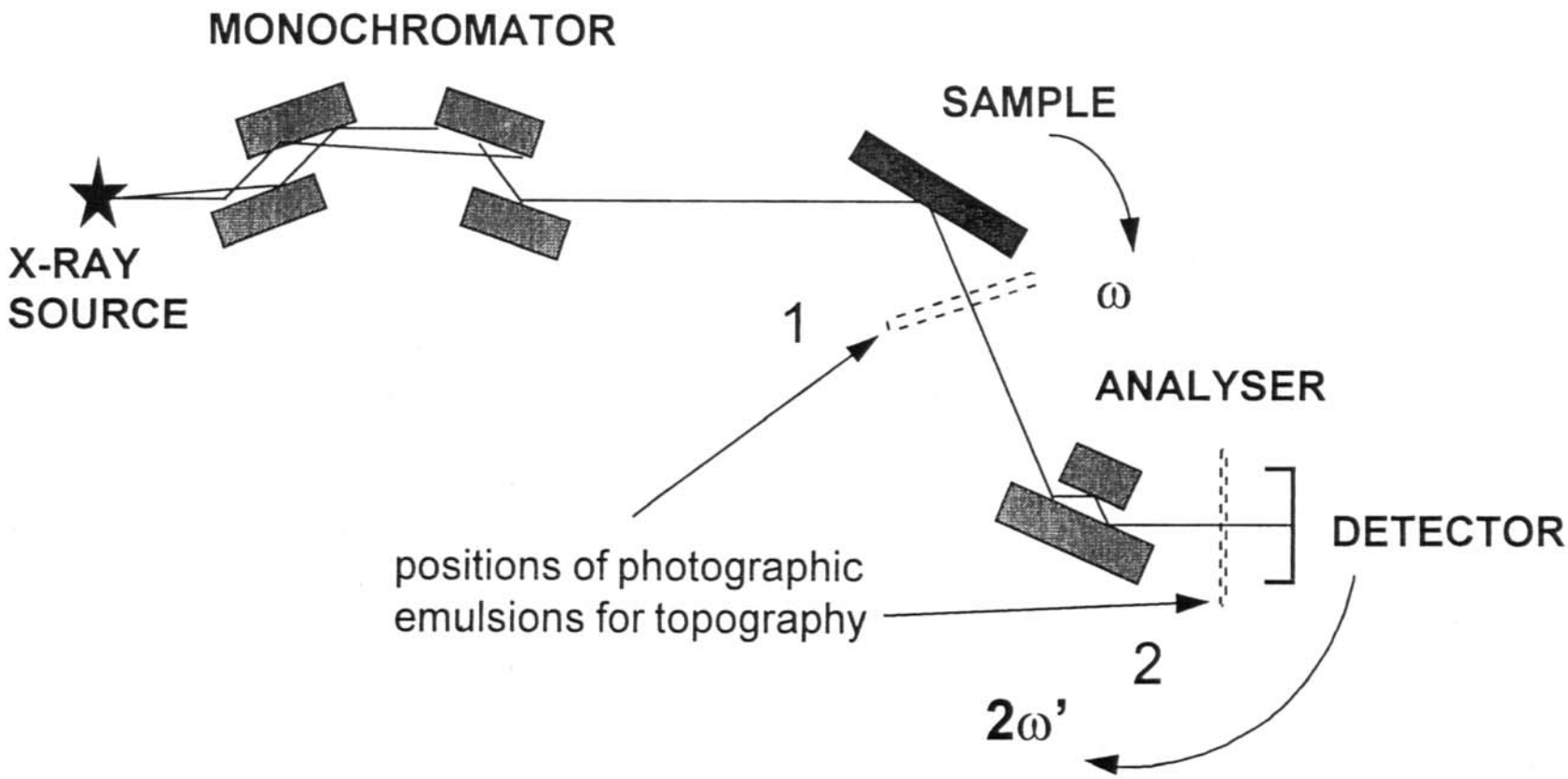

FIGURE 6. The geometry of the high-resolution multiple-crystal multiple-reflection diffractometer; this produces a well-defined and monochromatic incident beam and selects the scattered beam direction. This arrangement produces a very-well defined reciprocal space probe and can be used for topography and for absolute lattice parameter determination.

C. Absolute Lattice Parameter Determination

Placing the reciprocal space maps on an absolute scale allows the resulting diffraction pattern to be analyzed in much greater detail. The usual approach has been to use the substrate material as an internal standard, assuming that it is precisely unstrained, etc. Bond (1960) suggested a well-used method of determining the absolute lattice parameter by combining the results of the crystal reflection at two positions from the same set of crystal planes with the beam taking forward and reserve paths. This allowed very precise values to be obtained because problems associated with sample centering and zero errors were eliminated. This precise value could then be used to evaluate the scattering angle for the substrate material and hence put the diffraction space map (and hence the reciprocal space map) on an absolute scale.

The method of Bond becomes problematic with inhomogeneous or imperfect materials, because it relies on two measurements (slightly different sampling volumes) and the crystal rocking angle. Imperfect or bent samples will have a spread in crystal rocking angle, ω. Another approach was proposed by Fewster and Andrew (1995b) in putting greater reliance on the scattering angle that relates directly to the lattice parameter and can therefore cope with imperfect samples. This is a single measurement method and therefore also removes the complications of inhomogeneity. This latter approach takes into account simple geometrical considerations to overcome problems of sample eccentricity and incident beam alignment through the center of the goniometer. The instrument used was the high-resolution multiple-crystal multiple-reflection diffractometer (Figure 6), which is also used for high-resolution reciprocal space mapping. The principle of the method is simply that the $2\omega' = 0$ position can be determined to very high precision by moving the sample out of the incident beam and scanning the analyzer to achieve a very narrow profile that defines the incident beam direction. The high angular precision goniometer is then set to determine the scattering angle from the reflection of interest by moving the sample back into the path of the incident beam. The question of wavelength determination and diffracting plane alignment are all discussed by Fewster and Andrew. The accuracy will allow measurement of lattice parameters to within 1 ppm and is not restricted to perfect single crystals. This method has been demonstrated for imperfect mosaic crystals, layer structures, and polycrystalline samples. The essential aspect of this work is that now each position in a reciprocal space map can be placed on an absolute scale.

D. Applications of High-Resolution Reciprocal Space Mapping

Complicating diffraction features such as tilts and mosaicity can add to the difficulties in interpreting diffraction profiles. Reciprocal space mapping helps in this regard by separating the individual components. To obtain "perfect" agreement between a measured profile and the calculated diffraction profile even for "perfect" samples can prove troublesome and for modeling the scattering from partially relaxed layers can prove impossible using data from double crystal diffractometers. The problems of relaxation are considered later but for analysis of near perfect structures various diffraction effects require dynamical theory (Fewster and Curling,1987; Fewster, 1993), for example, in measuring thicknesses and compositions. Double crystal diffractometry in the conventional sense (Compton, 1917) cannot be used for reciprocal space mapping because the

probe is only defined in one direction. This, of course, has implications in the interpretation of the intensity profile obtained by the way in which the intensity is integrated in reciprocal space. Therefore, triple axis methods are preferable.

Triple axis techniques can in themselves create further complications because of the very high resolution inherent in the technique; this can lead to missing data of interest or the observation of subtle effects that can complicate the analysis (Fewster, 1993), although both these effects are resolved by limited area reciprocal space mapping and integration. Fewster and Andrew (1995a) have projected a reciprocal space map of a complex InGaAs/AlGaAs/GaAs laser structure onto a radial scan direction so that the profile intensity is solely dependent on the strain variation (the conventional variable used in dynamical diffraction theory). The resulting agreement between theory and experiment can be "perfect", that is, within the measured uncertainty and limits of the model. Similarly, the diffraction from superlattices can require the same treatment and to obtain detailed "perfect" fits to periodically δ-doped GaAs structures (Hart, Fewster, Ashwin, and Newman, 1995) had to project the data onto a radial direction. The resulting analysis gave the extent of the period variations (~1 monolayer) and δ-dope spreading by diffusion (<2 monolayers). These results are only possible by achieving a "perfect" fit.

1. Defect Analyses of Substrate Material

Imperfections in bulk crystals exhibit themselves as broadening of the diffraction profile, and for more subtle effects this will exhibit itself as diffuse scattering. The shape of the diffuse scattering can be related to the defect strain fields (Huang, 1947; Dederichs, 1971; Krivoglaz, 1969). Using reciprocal space mapping to study the diffuse scattering has several very clear advantages in that the diffraction from the perfect regions of the crystal can be separated from the weak diffuse scattering from the imperfect regions. However, the diffuse scattering is subject to dynamical diffraction interactions close to regions of strong scattering (Thomas, Baldwin, and Dederichs, 1971). Morilyansky and Garstein (1996) have used reciprocal space mapping to determine the distribution of diffuse scattering from defects in bulk InP. They separated the dynamical scattering by simulating the shape of the instrument probe and subtracted it from the pattern. Reciprocal space maps were collected in both reflection and transmission geometries. The conclusion from this is that the InP studied was composed of symmetric and antisymmetric components that could be interpreted in terms of vacancy loops occupying some of the {111} planes, whereas most of these planes are occupied by interstitial loops.

Of course, in reflection geometry the surface scattering can dominate the diffuse scattering. If the sample is poorly prepared, observations of the diffuse scatter can be a very effective means of studying surface treatments. Wang, Matyi, and Nordheden (1994) have studied the influence of surface preparation from reactive ion etching of GaAs by monitoring the diffuse scatter distribution measured in reciprocal space maps. The bombardment of ions in the reactive ion etching process leads to mechanical damage of the surface. This damage was assumed to be slight yet has been shown to have a dramatic effect on the diffuse scattering observable in reciprocal space maps. Wang et al. found that reactive ion-etched GaAs wafers reduced the level of diffuse scattering (defined in terms of its lateral extent) compared with those subjected only to chemical-mechanical treatment. When the ion

energy was increased the diffuse scatter no longer increased, suggesting that any damage occurred deeper into the wafer. The experiments were carried out on a (001) GaAs wafer with a 2° miscut and with the 113 reflection in grazing exit and CuKα radiation. The investigation of the diffuse scattering indicates that this is very sensitive and therefore is a very good technique for qualitative assessment. However, it is almost impossible to make this quantitative as with any interpretation of diffuse scattering. The reason being that the defects need to have an isotropic distribution or consist of dilute concentrations of similar defects.

The precipitation of native defects in semiconductor materials can have dramatic effects on the scattering and can therefore be a sensitive measure of the deviations from stoichiometry. Matyi, Melloch, Zhang, and Miller (1995) have studied the changes in the diffuse scattering as the As_4/Ga ratio was varied for different samples during growth of GaAs by low-temperature MBE. The diffuse scattering also became highly anisotropic for the As_4/Ga = 3.55 ratio. By modeling the reduction in diffuse scatter away from the Bragg peak, they determined an estimate of the precipitate sizes. These were estimated to be 200 Å and 420 Å for samples annealed at 700°C and 900°C, respectively. These values were 2 to 3 times larger than those determined by TEM, because the X-ray scattered intensity is sensitive to the strain induced as opposed to the precipitate itself. This study shows that in comparing analysis methods it is most important to understand the interpretative step. In the X-ray case of this example the scattering originates from deviations from perfection created by the precipitate, crystal plane rotation, and strain effects, which can extend long distances, whereas the electron micrograph determines the physical dimensions of the precipitate. However, the X-ray case is a large area average and that obtained by electron microscopy is an average of a very small region.

Fewster and Andrew (1993c) have examined the diffuse scattering from GaAs, Si, and Ge crystals with various states of surface preparation. The approach here was to try and identify the contributors to the diffuse scattering by topography. Because of the very small reciprocal space probe, the diffuse scattering could be probed very close to the Bragg peaks and any unwanted Bragg scattering would be excluded. The dimensions of the region sampled by the beam in this case was ~7 × 0.8 mm. The results suggested that much of the scattering comes from surface defects and dislocations with only a very weak background diffuse scattering coming from a homogeneous distribution of point defects and thermal diffuse scattering. It was only when the crystal perfection and surface perfection was of such a high quality that this more homogeneous background exceeded that of the individual defects.

Using this topography method very close to the strong diffraction peaks allows a large number of defects to be imaged because this region is most sensitive to very small deviations from perfection. This permits a rapid (~1 h exposure) topograph of the surface damage on the sample. Images could be made from many different regions of the diffuse scattering as observed in the reciprocal space maps, which indicated that certain parts of the strain and crystal plane orientation of each defect could be quantified. The advantage of this method is that the scattering imaged is solely from the regions of the sample that deviate from perfection and the parasitic scattering is negligible. Hence, the contrast does not depend on fluctuations in the Bragg scattering, as is the case with conventional topography.

Hu, Thomas, and Webjörn (1995) have used these topography methods to analyze subtle changes in the scattering caused by

periodically inverting the polarity of a bulk crystal of $KTiOPO_4$. These periodically poled domain structures are formed by either electron beam writing or by electric field poling; the former creates inversion through large depths (the thickness of the crystal), whereas the latter penetrates about 1 mm. The advantage of these structures is that they can operate as very efficient frequency doubling devices for lasers. The changes in the structure are minimal, that is, the Ti atom in the inverted domains undergoes a subtle change in site. This movement results in a subtle difference in intensity due to resonance scattering effects influencing the structure factor and microstructural changes. The microstructural changes are quite dramatic in the reciprocal space maps when comparing samples that have been modified and those that have not. An elongated region of scattering is observed along the [2-10] direction of a $LiNbO_3$ sample having a (001) surface plane. This mapping in combination with topography allowed them to interpret these changes as causing a "minutely misorientated" structure that they conclude arises from the strain induced from processing (piezoelectric effect). However, these strains are quite inhomogeneous and lead to the observed tilts evident as extended diffuse scattering in the reciprocal space maps. They have also detected a strain gradient at the boundaries of these domains, which was rather unexpected. An important point here was that they calculated the contribution to the anomalous scattering that gives rise to the potential intensity difference between the two regions is not influenced by crystal perfection, that is, the intensity ratio is the same in the dynamical and kinematical theory limit (Hu and Thomas, 1996).

2. Analysis of Mosaic Crystals

Examining gross imperfections such as mosaicity in the sample will show itself as a distribution of orientations and this was illustrated in Fewster (1991a), where significant orientations between the mosaic blocks was observed as a spreading in the rocking angle. A radial scan, on the other hand, suggested that the strain distribution in each block was small, producing a very good fit to theory. However, the lattice parameter did vary from block to block, which could be accounted for by the growth of this semiinsulating GaAs. In this case the block size was large and broadening of the profile from finite size effects was negligible. To confirm that the interpretation of the distributed intensity arose from contributions of individual mosaic crystal blocks, a series of topographs at various crystal rocking angles were taken to reveal the block size and images of the defects at the block boundaries. The size correlated with an anomalous transmission Lang topograph. A topograph taken while rocking the sample showed that the full sample region could be imaged and was composed of purely tilted blocks with small strain differences. The strain differences did indeed suggest that the lattice parameter decreased toward the edge of this liquid-encapsulated Czochralski grown sample as previously observed by Barnett, Tanner, and Brown (1985).

Of course, this orientation distribution of mosaic blocks, or for that matter any layer to substrate tilting of imperfect materials obtained with a double crystal diffractometer, can be very difficult to simulate. This is because the mosaicity and strain differences are not separated. On the other hand, a radial scan in triple axis mode may miss the tilted layer. However, a limited area reciprocal space map contains all the data necessary and by projecting the intensity onto a radial direction the contribution due to tilts, either in macroscopic form or microscopic form, can be retrieved (Fewster, 1991a). It must be remembered that a high-resolution diffractometer with an open detector integrates over a different region of reciprocal

space so only by judicious choice of reflection, etc., can comparable data be obtained.

3. Determining the Distortion in Si Layers on SiO_2/Si

To create an electrically insulated layer of Si, a popular approach is to create an oxide separating the layer from the Si substrate. However, the distortion of the layer may be of importance. Measuring the absolute lattice parameter of the layer and substrate in combination with the reciprocal space mapping can provide the answer (Fewster and Andrew, 1995b). This method has been used for determining the lattice parameters of a Si 1.2 μm layer separated from its Si substrate by a 2.5-μm oxide. The layer was tilted by as much as 650″ arc and 90″ arc in two orthogonal azimuths. The lattice parameter shows considerable correlation with the substrate, that is, it has a measurable tetragonal distortion. Although the maps are placed on an absolute scale, it must be remembered that the two-dimensional reciprocal space map is a projection, and therefore to obtain accurate values the layer and substrate diffraction planes had to be aligned separately. With relative diffraction plane tilting between the layer and substrate as in this example, the only reliable reciprocal space map for determining precision lattice parameters is with a three-dimensional reciprocal space map.

4. Determining the Relaxation in Layered Crystals

Fewster and Andrew (1993b) have used a combination of reciprocal space maps from several reflections to obtain detailed structural parameters of heavily relaxed InGaAs on GaAs. Also, they used the projection approach to recover all the intensity for modeling. The thicknesses and compositions were determined as well as the strain distribution close to the interface (Section IV.D.6). The highly disrupted and distorted lattice planes close to the interface contribute mainly to the diffuse scattering and are incoherent with the remainder. Incorporating this diffuse scattering into the model gave the interfacial strain. The reciprocal space maps also contain information concerning the microstructural components, mosaic spread and size and layer substrate tilts, and these were measured and plotted as a function of film thickness. The InGaAs compositions were all close to 5% In and the thicknesses ranged from 0.5 to 6 μm. The growth of this type of structure was intended to create the relaxed lattice parameters in the surface plane at the top of the buffer layer such that the subsequent $In_{0.10}Ga_{0.90}As$/GaAs superlattice would contain compressive and tensile strains and thus modify the electronic band structure. Only by doing a detailed analysis like this could the actual composition be determined of these partially relaxed structures.

The apparent mosaic spread decreased with increasing thickness along with an enhancement in the contrast of the topographs taken at the layer peak. The topographic features also reduced in size with increasing thickness above about 1 μm. This was explained in terms of the orientation spread in submicron level regions (below the dimensions of the topographic resolution) being large for smaller thicknesses. These regions then interacted to create regions of similarly orientated mosaic blocks. These mosaic blocks coalesce to form regions of smaller orientation spread, increasing the mosaic block sizes but reducing the size of these regions as the layer thickness increases. The mosaic blocks then finally dominate the structure; this was termed "the mosaic grain growth" model.

The considerable improvement in the analysis of strain relaxation using recipro-

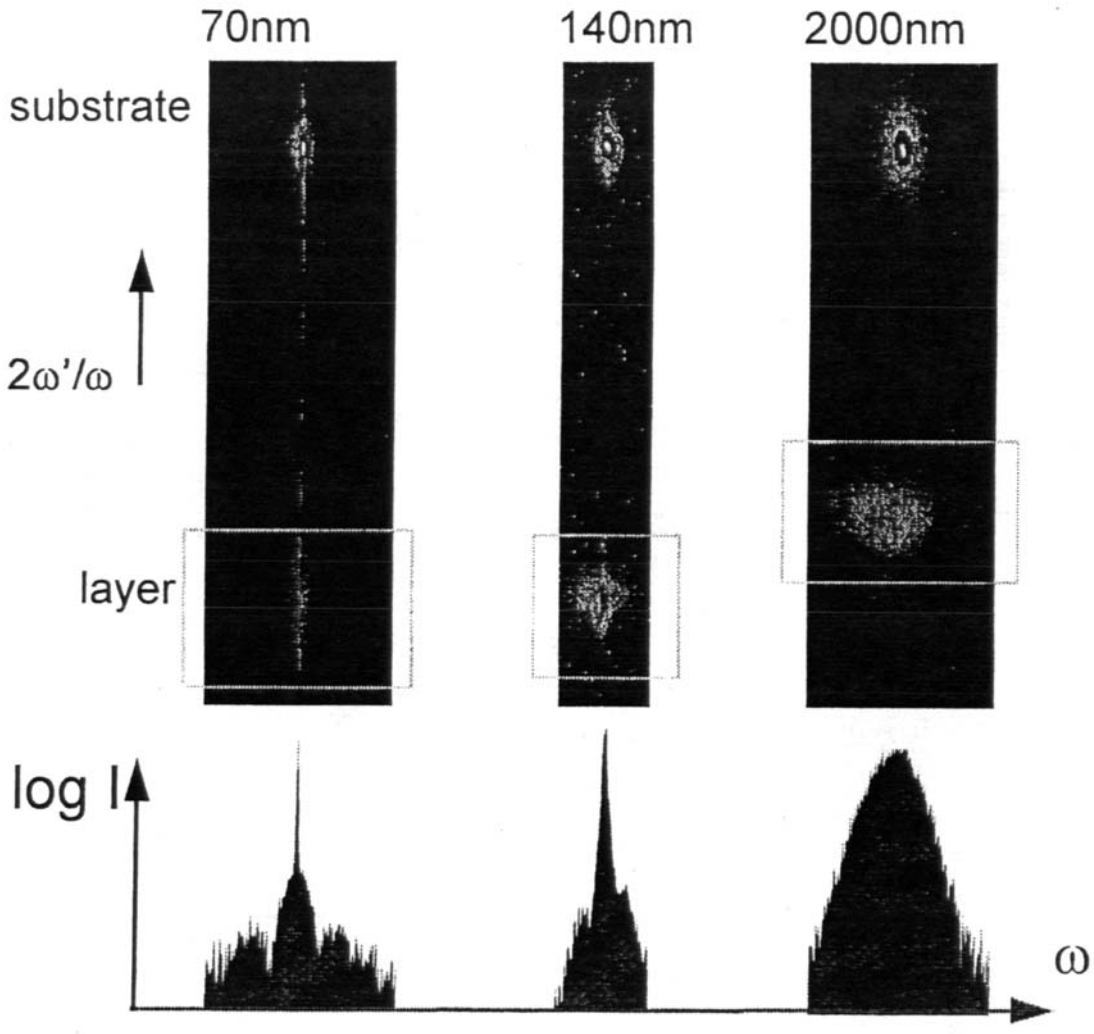

FIGURE 7. The change in scattering close to the 004 reflection for InGaAs layers of similar composition but of different thicknesses close to the critical layer thickness. The lower profiles show the integrated intensity scattered in the region of the layer peaks projected onto the direction perpendicular to the diffraction vector. This diffuse scattering can be interpreted in terms of the strain field dimensions of the dislocations at the interface.

cal space maps compared with double crystal diffaction profiles has been demonstrated by Koppensteiner, Ryan, Heuken, and Söllner (1993) for ZnSe layers on GaAs. In this study they showed that the deviations can be very large, especially for small relaxations, and clearly indicates the sensitivity of the method.

The onset of relaxation is important to understand because the introduction of defects to relieve the high internal stress levels can have a serious detrimental effect on the subsequent electronic device performance. The early stages of relaxation are very subtle and have been observed by imaging the dislocations in X-ray topography (Eaglesham, Kvam, Mayer, Humphreys, Green, Tanner, and Bean, 1988). Similarly, the influence of these dislocations can be studied by reciprocal space mapping by observing the diffuse scattering (Kidd, Fewster, Andrew, and Dunstan, 1993). The diffuse scattering in this case was interpreted directly from the reciprocal space maps. A series of $In_{0.09}Ga_{0.91}As$ layers of different thicknesses straddling the abrupt change in the thickness/residual strain relationship were analyzed.

At the early stages of relaxation it was observed that weak diffuse scattering begins to increase close to the layer peak, initially in the form of lobes that eventually coalesce into an ellipse as the layer thickness increases. The layer peak of the 004 reflection from a (001)-orientated sample was found to broaden normal to the diffraction vector due to the decreasing lateral correlation length of the unperturbed regions of the layer, while the diffuse scatter profile initially became sharper (Figure 7). Eventually, as the thickness increases the two contributions became indistinguishable, elliptical shaped, and their lattice parameter appeared to collapse. The extent of the elliptical form gradually decreased in size with increasing thickness in common with the observations of Fewster and Andrew (1993b).

The scattering in the vicinity of the layer peak was projected onto a plane normal to the diffraction vector to obtain the lateral dimensions of the correlation lengths contributing to this scattering. Kidd et al. have correlated these lengths with the layer thickness and see a clear relationship that indicates the distortions from misfit dislocations extend as far as the nearest geometrical constraint that will relieve the strain. Hence, a thin layer sample with dislocations that are well separated appear to have their distortion strain fields relieved at the sample surface, and this restricts their lateral extent. As the dislocation density increases, the geometrical constraint becomes the strain field overlap laterally, and therefore this restricts its extent normal to the interface.

The diffraction from these samples have been modeled after projection of the reciprocal space maps onto the radial scan direction to reconstruct the interface distortion and by combining this with the lateral correlation length dimensions the average microstructures could be determined (Kidd and Fewster, 1994; Kidd, Fewster, and Andrew, 1995). These results were also corroborated with plan view transmission electron micrographs, where the dislocation separation was measured for all four samples. The thinner layer samples of 700 and 1400 Å thickness gave a peak in the distribution of separations well below the layer thicknesses; in fact, 90% and 74% of the separation lengths were in excess of the layer thicknesses, respectively. For the 2000- and 4000-Å-thick layers, the number of separations in excess of the layer thicknesses were 13% and 0%, respectively. These distributions became narrower with increasing thickness. These results of two analytical approaches therefore corroborate. It was also clear from this study that the mean dislocation separations do not correspond to the mean distance of a regular array. Therefore, counting dislocations will give an unreliable value for the strain

relaxation without including their distribution, because any dislocation bunching will reduce the effective strain relief.

5. Relaxation Determination by Routine Analysis Methods

Heinke, Einfeld, Kuhn-Heinrich, Pahl, Möller, and Landwehr (1995) have used the approach of Heinke, Möller, Hommel, and Landwehr (1994) to try and simplify the analysis of relaxing structures of II-VI compound semiconductors. Basically, they show from simple geometrical considerations that the locus of variable relaxation and composition have different directions in reciprocal space and can therefore be separated. The reciprocal space map of a CdMgTe layer on a (001) CdTe substrate was analyzed from which they could conclude that the layer has a strain gradient, that is, variable relaxation, from the direction of the broadening. This rapid analysis approach is applicable to isotropic strain in the layers but does not include the complications of mosaic block size effects and their relative orientations. However, as an approach for rapid screening of material this could prove to be a good procedure.

The combination of reciprocal space mapping and the use of the absolute lattice parameter method has allowed very precise determination of the unit cell parameters of a relaxing layer and those of its substrate (Fewster and Andrew, 1996b). The principle of the technique relies on the fact that the goniometer used has very precise optical encoding on both the ω and the $2\omega'$ axes, and therefore all the reciprocal lattice points can be interrelated on a relative as well as an absolute scale. This enables the possibility of deriving the lattice parameters parallel and perpendicular to the interface plane with equal precision. Because the absolute lattice parameter method of Fewster and Andrew (1995b) has the capability of determining the lattice parameters to within a part per million, the determination of the relaxation parameters can be very reliable. A consequence of this study also indicates that the use of the substrate as an internal standard can lead to significant errors, because significant strain extends down into the substrate that is not uniform. This can result from the epitaxy itself and be complicated further by the process of relaxation. The judicious choice of reflections with similar penetration depths therefore becomes very important.

6. Interface Analysis of Relaxing Layered Structures

Recovering the full intensity, as described above, allows the modeling of the intensity profile in terms of strain or deviation parameter in dynamical theory (Fewster, 1992). Of course, the coherently scattered intensity is recovered along with the incoherent or diffuse component. In general, this is small unless a significant number of defects are present. For epitaxial layers that have started to relax, a high level of mosaicity and diffuse scattering is present, and the interpretation of such structures requires modifications to dynamical theory Kato (1980) for general distributed defects and Fewster (1992) for interfacial defects. Kato introduced the idea of limited coherence lengths of X-ray wavefields in a crystal with defects that showed a route to analyzing imperfect structures. Fewster used these ideas and modeled the projected profiles of measured reciprocal space maps. These maps contained the distribution of scattering due to mosaicity and diffuse scattering, as well as the dynamically scattered contribution. These profiles projected onto the radial direction were compared with the calculated profile that is based on coherence breakdown and strain

gradients. From this it was possible to estimate the extent of the distortion of the interfacial region and correctly determine the layer thicknesses. The scattering is considered purely dynamically, although the various contributions have to be considered individually and recombined in terms of their various phase relationships. In general, the distribution of different paths results in a phase averaging effect, and this has the appearance of phase incoherence between the different paths for the X-ray photon. For a single interface the scattered intensities is given by:

$$R(w) = \left[(1-\Omega)X_{perfect} + \Omega((1-\xi)X_{above.defects} + X_{below.defects}\right]^2 + \left[\xi X_{above.defects}\Omega\right]^2 + \left[\Omega X_{defects}\right]^2$$

where Ω is the proportion of the sampled region disrupted by defects and ξ is the proportion of the scattering from above the defects that is coherent with that from below. X represent the scattered amplitudes from the various regions. The amplitude from the defected region was calculated on the basis of an extended disrupted region scattering and appeared, for example, as the "wings" in Figure 8.

Without taking into account the influence of dislocations at the interface, in this way the magnitude of the scattering in parts of the profile could result in considerable errors. However, the distribution of scattering in the reciprocal space maps only requires a very low concentration of interfacial defects (one dislocation per 10 μm) to create significant "ears" on the substrate peak shape (Figure 8). The "ears" are at higher scattering angle with a spread in crystal rocking angle (ω) and can be explained as the regions remote from the dislocation core, where the diffracting planes are bent (spread in ω) and exist in regions of lower

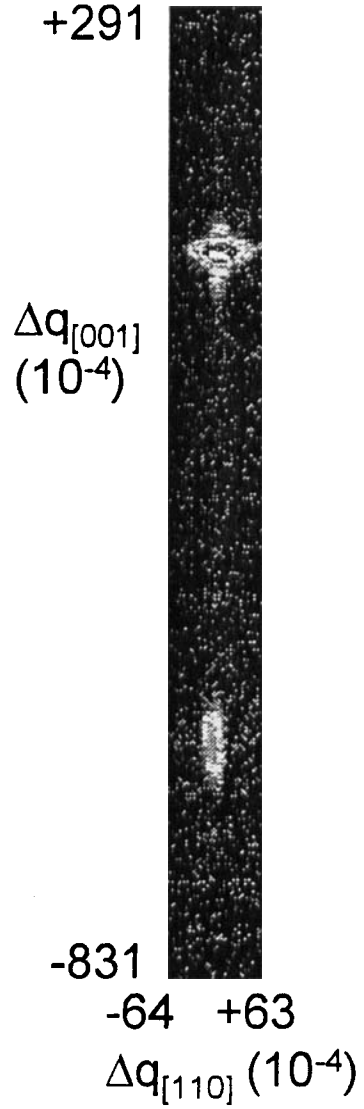

FIGURE 8. The distribution of scattering close to the 004 reflection from a SiGe layer and Si substrate. The extended intensity close to the substrate peak is that which arises from the interface distortion as dislocations are present that rotate (creating a spread in $q_{[110]}$) and collapse the planes parallel to the surface (increase the value of $q_{[001]}$) within the substrate.

lattice parameter. These observations are explained by the right-hand diagram in Figure 9. The substrate in this region has been stretched laterally, and therefore the lattice parameter has collapsed vertically due to the Poisson effect in an attempt to match the

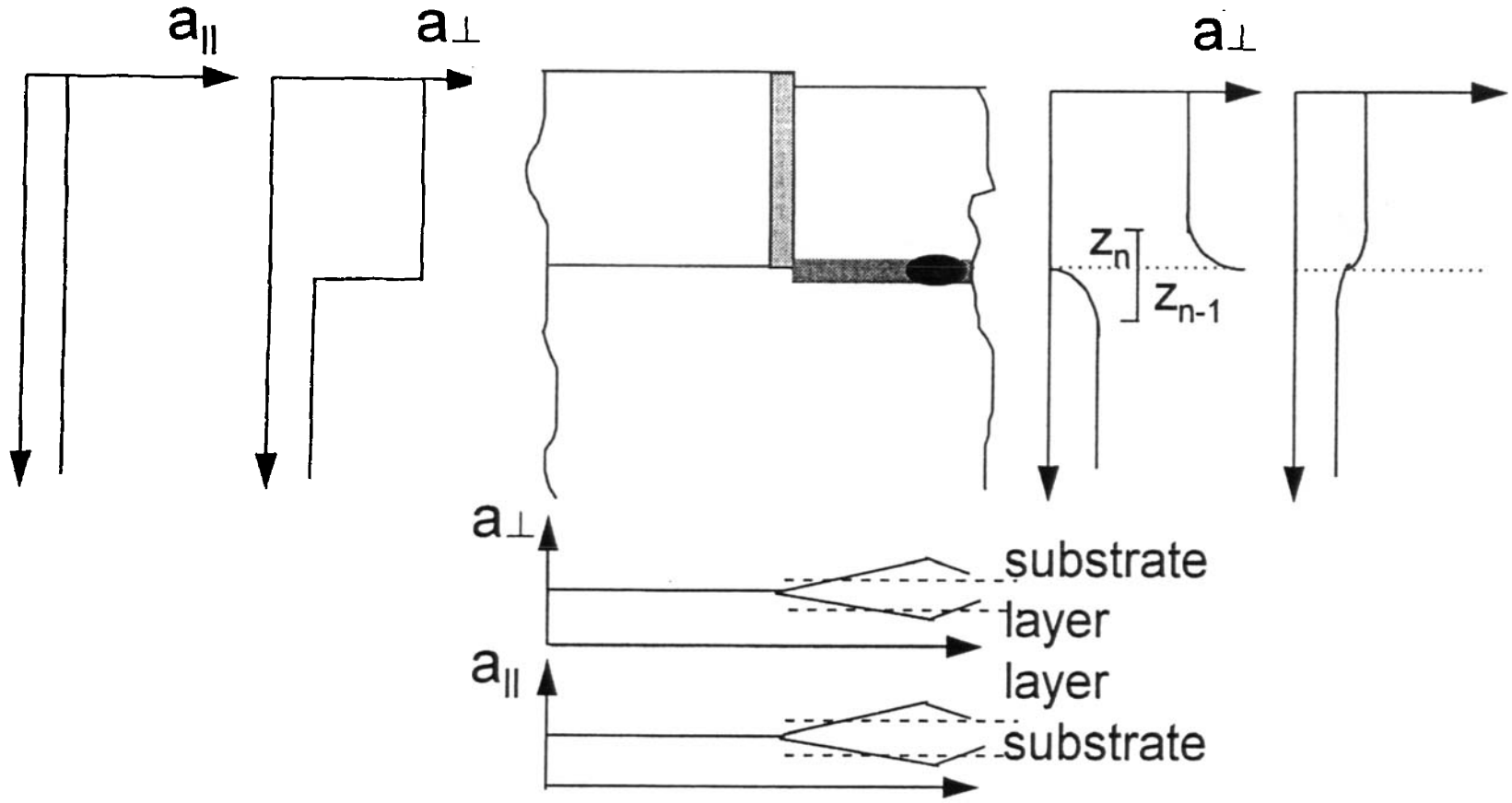

FIGURE 9. The variation in lattice parameters close to the interface due to the presence of dislocations. The lattice parameter parallel to the ir becomes discontinuous and varies as a function of depth due to the dislocations. The perpendicular component is influenced by the Poisson effect. The variation in the lattice parameters also influences the scattering and should be included when simulating the scattering.

partially relaxed layer lattice parameter. It is these distortions that are determined in the model of Fewster (1992). The cross-hatched array of dislocations were also clearly revealed by topography at various positions in the reciprocal space map. This diffraction model therefore reveals the interfacial strain resulting from misfit dislocations and more fundamentally simulates the scattering from the individual layers correctly to derive their thicknesses and compositions correctly.

7. Direct Approaches to the Interpretation of the Diffuse Scattering

Clearly, the diffuse scattering created from a partially relaxed structure results from several contributions, that is, mosaic block size and tilts between mosaic blocks. Fewster (1996b) has taken a simple approach to directly interpret the diffuse scattering and separate these two components. In general, the mosaic blocks in a relaxing structure are approximately disc shaped with a characteristic lateral width (lateral correlation length) parallel to the interface. This lateral correlation length creates a broadening parallel to the sample surface, whereas the tilting (provided each block has a comparable lattice parameter) creates a broadening perpendicular to the radial scan direction. By measuring the angle that the diffuse scattering ellipse makes with respect to the radial direction and its width, L, these two contributions can be separated and determined using the following formulae:

$$\text{microscopietilt} = -L\frac{\cos(\phi+\xi)}{\sin\phi}$$

where ξ is the angle that the axis of the ellipse makes with the radial direction ($<\pi/2$) and ϕ is the angle between the surface normal and the diffracting plane normal.

$$\text{lateral-correlationlength} = \frac{\lambda}{\sin[2\omega'-\omega](\Delta 2\omega'-\Delta\omega)-\sin\omega\Delta\omega}$$

where

$$\Delta\omega = L\frac{\cos\xi}{\sin\phi}(\cos\phi+\sin\phi\tan\theta)$$

and

$$\Delta(2\omega') = L\frac{\cos\xi}{\cos\theta}$$

and ω and $2\omega'$ represent the angle that the incident beam makes to the sample surface and the scattering angle, respectively. Clearly, by mapping the intensity from a diffracting plane that has a large angle with respect to the surface plane (i.e., large ϕ), then it is possible to obtain the most accurate value for these parameters. To indicate the size of these various contributions consider Figure 10, then the contribution giving rise to the microscopic tilt is about half that due to the contribution from the finite lateral correlation length. These contributions amount to 22″ arc and 6180 Å, respectively. Therefore, it is important therefore to separate these two components before deriving too many conclusions regarding the microstructure directly from reciprocal space maps. This method assumes that the strain distribution as a function of depth is small. This can be judged by the width of the radial scan profile for diffraction planes parallel to the surface compared with theoretical widths.

Goorsky, Meshkinpour, Streit, and Block (1995) have taken a very pragmatic route to analyzing the diffuse scattering and related

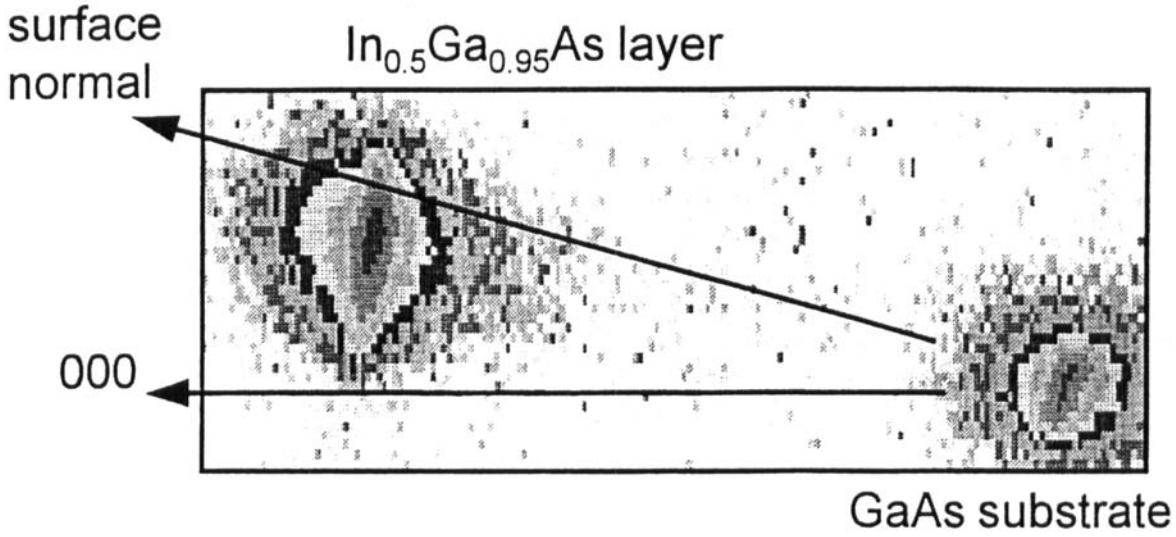

FIGURE 10. The scattering from a thick InGaAs layer that has relaxed significantly, 115 reflection. Because the axis of the diffuse scattering from the layer profile is not aligned in a direction normal to the surface normal or the direction to the origin of reciprocal space, it contains both finite size effects and distributions of orientations. These can be separated.

the intensity and shape to semiconductor device performance. In this case they just studied the diffuse scattering close to the substrate peak as this simplified the alignment and the diffuse scattering was strongest in this region. They observed that the diffuse scattering from a HEMT structure was much stronger when the diffraction plane is normal to the [–110] direction and considerably weaker when normal to the [110] direction. The asymmetric distribution of dislocation densities observed by electron microscopy confirmed this. Goorsky et al. attributed this diffuse scatter to arise from lattice tilts and concluded that this scatter is sensitive to misfit dislocation levels below 0.3 μm^{-1} with the intensity having a linear relationship with dislocation density. This can obviously be a rapid screening method for analyzing devices.

8. Modeling Reciprocal Space Maps of Relaxing Layered Crystals

Kaganer, Köhler, Schmidbauer, Opitz, and Jenichen (1996) have used the correlation function derived by Krivoglaz (1969) based on Poisson statistics for uncorrelated dislocation strain field interaction and the Kubo cumulant expansion for positional correlations to model these reciprocal space maps. Krivoglaz proposed that the diffraction from a distorted crystal can be entirely determined by the correlation function:

$$G(\mathbf{r}.\mathbf{r}') = \langle \exp(2\pi i \mathbf{h}.[\mathbf{u}(\mathbf{r}) - \mathbf{u}(\mathbf{r}')] \rangle$$

where $\mathbf{u}(\mathbf{r})$ is the random atomic displacement and $\mathbf{h}$ is the scattering vector. The averaging is over all configurations. The Fourier transform of this function then gives the distribution of intensity in reciprocal space.

Kaganer et al. assume that the elastic parameters of the two components of the bicrystal are identical and assumed that the distortion field extended into the layer. The problem was treated kinematically and because the distortion field was assumed to be identical in the layer and substrate only the scattering from the former was considered. Also, it was assumed that the coherently diffracting con-

tribution was very small. They showed from this theoretical approach that the diffraction maximum followed the mean distortion for large dislocation densities in agreement with Chu, Macrander, Strege, and Johnston (1985) but was not the case for small dislocation densities, as can be observed in Figure 8. The shape of the scattering in reciprocal space for edge and 60° dislocations on (001)-orientated samples was calculated to be quite different, that is, the $\Delta q_{\parallel}/\Delta q_{\perp}$ ratio of these elliptical shapes were 0.68 to 0.3, respectively.

For their calculations of large mismatches, the comparison with experimental results suggested that the dislocation distortions were correlated and an additional parameter was required. The complexity was increased further if both edge and 60° dislocations coexist. For lower dislocation densities both coherent and incoherent contributions coexist and using the same approach Kaganer et al. were able to reproduce the satellite reflections illustrated in Figure 8. Their model also predicts that they will not exist for edge dislocations. The experimental reciprocal space maps were compared with theory and the agreement was in fairly good quantitative agreement for AlAs/GaAs structures, although problems of anisotropic elasticity could account for some of the discrepancies with the studies on SiGe structures. For a high dislocation density SiGe sample, the observed profiles were greater than that calculated and could be accounted for by including a nonuniform distribution of tilts. An AlSb/GaAs structure also with a high-dislocation density gave a very poor fit and could only be accounted for by introducing a very strong position correlation between the dislocations. It is clear from this work that this is a useful route to simulation of the diffuse scattering and consequently the evaluation of the nature of the dislocation structure in these materials.

Another study making use of the kinematical theory with statistically distributed misfit dislocations of Krivoglaz (1969) and Peterson and Kaganer (1994) has been carried out by Holy, Li, Bauer, Schäffler, and Herzog (1995). From this modelling, Holý et al. were able to estimate the strain profile and the misfit dislocation densities. The influence of threading dislocations in all these studies was assumed to be small. Again, this approach was valid provided that the dislocation density was not too large because they assumed that $|\mathbf{r}-\mathbf{r}'|$ was small compared with the separation between dislocations as this simplifies the determination of the probability distribution of the separation distances. It was recognized also that if there was significant dislocation interaction the Gaussian distribution of separations and intensity were not necessarily valid. However, it was shown that this neglect only results in a small (10%) error in the statistical variable $c(\mathbf{r})$ in the calculation of the random atomic displacements:

$$u_i(\mathbf{r}) = \sum_{\mathbf{R}} w_{if}(\mathbf{r}-\mathbf{R})b_j c(\mathbf{R})$$

where b_j is a component of the Burgers vector and w_{ij} is the distortion at point $\mathbf{r}$ from a dislocation passing through the lattice site $\mathbf{R}$. To account for the inhomogeneity in the distortion, the epitaxial layer was considered as a series of homogeneous sublayers. Holý et al. measured the reciprocal space maps of the 004 and 224 reflections of a SiGe sample to estimate the misfit dislocation density and the average layer strain. Although the diffuse scattering was weak, reasonable agreement with theory was obtained and the discrepancies that do exist are thought to arise from exclusion of the contribution due to threading dislocations.

Koppensteiner, Hamberger, Bauer, Holý, and Kasper (1994) have considered the diffraction from a SiGe superlattice that diffracts coherently throughout its depth but has a finite correlation length of 400 Å normal to this direction. They considered two

structural models; one assumed that the mosaic blocks were disc shaped, perfect within themselves, each having a statistically determined tilt with respect to its neighbor and the second model was based on spherical blocks. Although the study was rather inconclusive concerning the actual shape of the mosaic blocks Koppensteiner et al were able to determine the dimensions of the laterally coherently diffracting regions in the sample.

9. Modeling the Diffuse Scattering to Study Threading Dislocations

Kyutt, Ruvimov, and Argunova (1995) have combined reciprocal space mapping in Bragg (reflection) and Laue (transmission) geometries. From these maps they were able to determine the relaxation extent of each SiGe sublayer in a heterostructure multilayer by comparing $(\Delta d/d)_{\parallel}$ and $(\Delta d/d)_{\perp}$. The relationship between these values gave a good indication of the concentration of misfit dislocations. The relative depths of the these arrays were also determined by calculating the individual layer thicknesses from the integrated intensities. Kyutt et al. concluded that the misfit dislocations broadened the profiles normal to the scattering vector (from planes parallel to the interface), while threading dislocations create a more general broadening in normal and parallel directions.

As mentioned previously, the determination of threading dislocation densities is more difficult than for misfit dislocations, primarily because the diffuse scattering is more isotropic and distributed. Early X-ray diffraction methods for obtaining these values was through measuring the profile widths obtained in double crystal diffractometry, although agreement with electron microscopy is generally poor (Gay, Hirsch, and Kelly, 1953; Jäger, Stenkamp, Ehrhardt, Leifer, Sybertz, Kibbel, Presting, and Kasper, 1992). This lack of agreement arises from the uncertain distribution of threading dislocations. Koppensteiner, Schuh, Bauer, Holý, Watson, and Fitzgerald (1995) have approached the determination of the threading dislocation density by calculating the total energy density due to random strain fields and subtracting the misfit dislocation density contribution, such that the density of threading dislocations is given by:

$$\rho_{ThreadingDislocations} = \frac{(E_{RandomStrains} - E_{MisfitDislocations})}{\left(\frac{E_{ThreadingDislocations}}{L}\right)}$$

where E represents the energies involved and L the threading dislocation line length. The energy terms and Burger's vector and the radii of influence of the distortion field need to be known, but because these are functions of the dislocation density, the denominator is unknown and the process becomes iterative. Koppensteiner et al. have modeled the scattering from 004 and 224 reciprocal space maps with various models and concluded that dislocation densities can only give an upper limit value because the agreement with EBIC indicated a large discrepancy.

10. Reciprocal Space Mapping of Superlattice Structures

The analysis of superlattice structures has a significant advantage in obtaining information about the interfaces. If the satellite reflections that result from this periodicity have a different shape in reciprocal space than the "average" superlattice reflection, then this could very well be from the finite correlation lengths associated with the roughness (Fewster, 1991b). A simple measure of this profile width for each satellite order could then probe the interface in great de-

tail. However, even from this analysis of this diffuse scattering from the first-order satellites, an asymmetry was observed that indicated that the correlation length in the ⟨110⟩ direction was half that of the ⟨1-10⟩ direction and qualitatively agreed with results from a scanning tunneling microscope study. Holý (1994) has proposed a theoretical approach to estimate the various contributions to imperfections in superlattices, including mosaicity, strain gradients, and in-terfacial roughness. The principle of the correlation length contribution to the diffuse scattering is as described earlier, except in this case the roughness can be correlated from layer to layer. The correlation function associated with the mosaic structure is as given previously; however, the interfacial roughness can be treated as a fractal surface (Sinha, Sirota, Garoff, and Stanley, 1988).

$$G_j(\tau) = \sigma^2 \exp\left[-\left(\frac{\tau}{\Delta}\right)^{2h}\right]$$

for the j th interface, where τ is the distance over which the correlation in the interface plane is considered, Δ the correlation length, σ the root-mean-square roughness, and h the fractal parameter. For the correlated roughness, Holý took the root-mean-square-roughness to be given by $\sigma(N - j)^{0.5}$, where N is the number of layers and the substrate surface was assumed to be ideally flat. The differences in the diffuse scattering from uncorrelated and correlated roughness was very dramatic; the former resulted in narrow profiles in $\omega/2\omega'$ and broad profiles in ω, whereas the latter resulted in a more general, rounded profile in the reciprocal space maps. Additional influences of strain effects can also contribute to the shape of the diffuse scattering by elongating the shapes along the scattering vector.

11. Laterally Periodic Structures Studied by Reciprocal Space Mapping

The analysis of complex quantum wire and dot array structures is greatly enhanced by the use of reciprocal space mapping (Gailhanou, Baumbach, Marti, Silva, Reinhart, and Ilegems, 1993; van der Sluis, Binsma, and van Dongen, 1993). This greatly improves the possibilities of interpreting the various periods, geometrical shapes, strains, damage, and compositions within the structure. Van der Sluis et al. modeled the reciprocal space map using a simple Fraunhofer approximation, whereas Gailhanou et al. also included other diffraction effects in the kinematic approximation. This more complete modeling included all the incident, transmitted, and transmitted diffracted beams to account for the subtleties in the diffraction pattern. If the etching of the structure reaches below the layer depth, additional satellites will be observed centered around the substrate peak as well as that of the layer (Tapfer, Sciacovelli, and De Caro, 1995; Darhuber, Koppensteiner, Bauer, Wang, Song, Sotomayor-Torres, and Holland, 1995). Darhuber et al. have also observed that the finite thickness fringes associated with the layer did not correspond to the expected thickness and concluded that the top of the wires were very imperfect and were not contributing to the scattering. A large peak shift of the residual layer wires was also observed and was thought to arise from inclusion of ions during the reactive ion-etching process.

V. FULL THREE-DIMENSIONAL RECIPROCAL SPACE MAPPING

A. Principle and Method

It must be realized that all data collection methods assign an integrated intensity

to a specific set of coordinates in reciprocal space. If the reciprocal space probe is defined rather precisely, then the measured intensity at any position can be assigned to small and specific angular ranges, thus making interpretation that much more meaningful. Three-dimensional reciprocal space mapping, and to a lesser extent two-dimensional reciprocal space mapping, therefore improve on the probe of the double crystal diffractometer that defines the probe angular only in one direction.

The importance of three-dimensional reciprocal space mapping can best be understood by considering a reciprocal lattice point (or the optimum diffracting condition for measuring the intensity) that is tilted out of the plane of the diffractometer. Its position moves in an arc such that any movement out of the diffractometer plane will increase the "apparent" crystal rocking angle (ω) and will increase the "apparent" scattering angle ($2\omega'$) if $2\omega'$ is greater than $\pi/2$ and decrease the "apparent" $2\omega'$ if it is less than $\pi/2$. Hence, to obtain reliable quantitative results this must be realized or minimized experimentally by reducing the axial divergence. These movements have been used for obtaining automatic alignment procedures to bring the diffracting plane of interest into the optimum diffracting condition (Fewster, 1985). Restricting the reciprocal space probe in three dimensions (axial and horizontal divergence, detector acceptance angle, and wavelength dispersion) allows reciprocal space mapping in three dimensions. This can produce a three-dimensional reciprocal space representation of a reciprocal lattice point. Three-dimensional diffraction space mapping effectively removes problems of alignment because the axial divergence limits diffraction to a region close to the diffractometer plane.

The resolution so far has only been considered in the plane of the diffractometer; however, the axial divergence is also very important when interpreting the reciprocal space maps. The "conventional" reciprocal space map is a projection of the measured intensity onto the diffractometer plane. By restricting this divergence to small values, Fewster and Andrew (1995a) have shown that it is possible to obtain the full three-dimensional shape of the scattering. It is very difficult to extract reliable quantitative data from two-dimensional reciprocal space mapping when dealing with imperfect material, for example, for a small change in the tilt alignment the apparent lattice parameter difference of individual mosaic blocks can be reversed. However, for example, three-dimensional reciprocal space mapping allows a very complete analysis of the quality of the epitaxy. This method shows considerable promise; however, what is perhaps more important at this stage is to be aware that the resolution function is a three-dimensional shape and a two-dimensional reciprocal space map is a projection of the scattering from a curved surface onto a plane.

As discussed in the introduction, the diffraction from a three-dimensional sample will create a three-dimensional diffraction pattern, and any representation of dimensions less than this must necessarily be a projection. Of course, even the size of the diffraction probe will result in an integration of the scattering close to the measured point and assign it to that point; however, this is just the instrument-smearing function that is always present. The extent of the smearing in three dimensions is necessary to understand the true location and magnitude of the scattering. It is clear, therefore, that a single rocking-curve obtained with a double-crystal diffractometer, for example, associates a significant distribution of scattering in reciprocal space to one point. The conventional (two-dimensional) reciprocal space map essentially has a well-defined probe in two dimensions and therefore is purely a projection of the integrated scattering onto a plane. A three-dimen-

sional reciprocal space map has a better defined third dimension and therefore the assumptions are reduced further. This method was first used by Fewster and Andrew (1995a) to interpret the scattering from mosaic structures so that reliable misorientations and lattice parameters could be obtained.

B. Applications of Three-Dimensional Reciprocal Space Mapping

All the studies described in the following sections make use of the high-resolution diffractometer illustrated in Figure 6. The axial divergence is modified with slits in both the incident and diffracted beam paths.

1. Mosaic Blocks

Fewster and Andrew (1995a) used this approach to interpret the diffraction from a mosaic semiconductor sample to obtain absolute lattice parameter values of individual mosaic blocks and to observe deviations from perfect epitaxy in terms of relative tilts. The sample was of an AlGaAs layer grown by MBE on a mosaic semiinsulating GaAs substrate. The area studied consisted of three mosaic blocks that were observed by two-dimensional reciprocal space mapping. However, depending on relative positions of their reciprocal lattice points to the plane of the diffractometer their apparent positions were displaced (Figure 11). The reason for this is that the diffraction probe is not linear in reciprocal space and therefore the projection can give rise to a complete misinterpretation of the reciprocal space maps.

The three-dimensional reciprocal space map therefore resolves this so that the true positions of the reciprocal lattice points for each mosaic block can be determined. Fewster and Andrew were therefore able to show that each block has a different lattice parameter and that only small relative tilts were observed between the substrate and layer. It is also interesting to note that the shapes of the layer reciprocal lattice points follow those of the substrate very closely (Figure 12).

2. Polycrystalline Material

These methods have also been applied to polycrystalline material (Fewster and Andrew, 1996a). The measurement of microstrain is conventionally performed using a slit based powder diffractometer by comparing reflections from parallel planes but of different orders such that the differences in profile width can be related to the "microstrain" (Warren and Averbach, 1950; Williamson and Hall, 1953). The question of interest to Fewster and Andrew was whether the individual crystallites contained a distribution of strain, that is, true microstrain or whether each crystallite had a different strain value. The two methods were also compared. A three-dimensional reciprocal space map of a textured Al sample is given in Figure 13. The shape of this Debye-Scherrer ring is obviously very complex because at this resolution the scattering from individual crystallites could be partially isolated. It must also be remembered that the lattice parameters of each crystallite can be placed on an absolute scale (Section IV.C), and therefore the distribution of orientation texture and distribution of strain is all contained in this map.

The size of the crystallites determined from this map were ~4 μm because the diffraction widths were close to the intrinsic instrumental broadening of 7″ arc at this scattering angle. Provided that the distribution of strain within an individual grain is

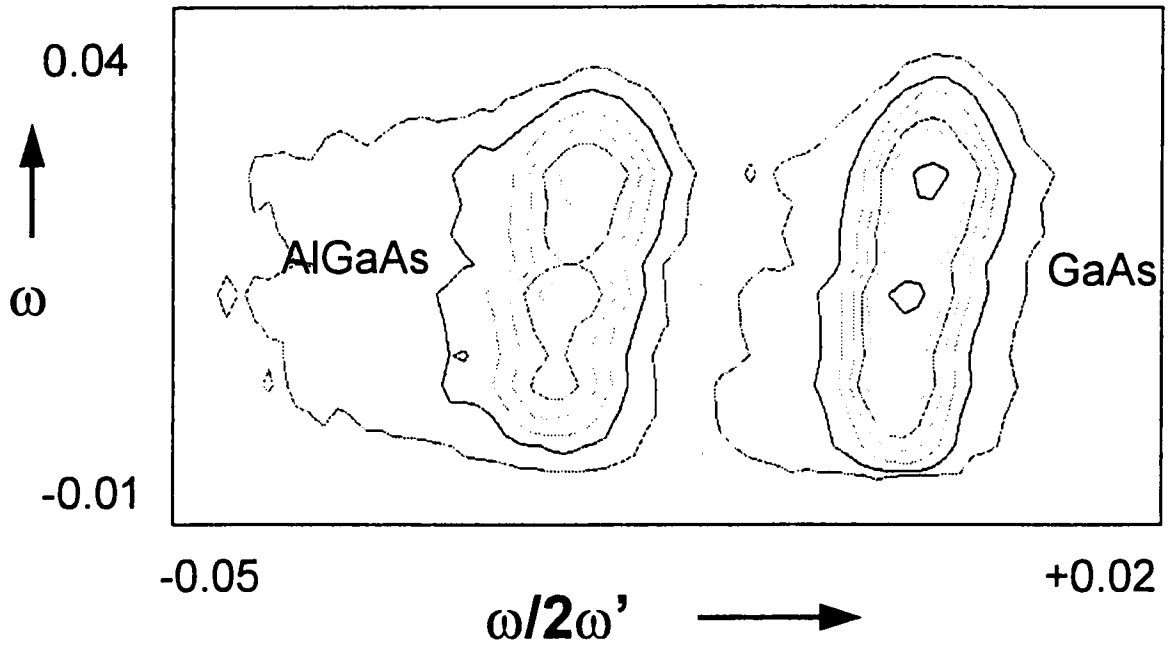

FIGURE 11. The two-dimensional reciprocal map from a mosaic GaAs layer with an AlGaAs layer. The data indicate three clear mosaic blocks in the substrate that is mimicked in the layer. Yet, obtaining relative tilts and lattice parameters is fraught with difficulties, as explained in the text.

less than ~8×10^{-5}. The main strain distribution is clearly observed as individual crystallites having their own value distributed about a mean. The two arms of the Debye-Scherrer ring have significantly different lattice parameters, and the weighted average compares with that obtained by conventional powder diffractometry. These studies were all carried out in high resolution.

3. Analysis of Protein Crystals

Reciprocal space mapping has been applied not only to strongly diffracting semiconductor samples and polycrystalline samples but also to protein crystals. Good-quality protein crystals are notoriously difficult to grow and also are extremely weak scatterers. The crystal quality ultimately determines the real space resolution achievable with X-ray diffraction for determining the molecular structure (Helliwell, 1988). There are complications of limited crystal size, shelf-life, and degradation in the X-ray beam. Attempts to improve the understanding and to produce higher quality crystals have been carried out in space to achieve microgravity conditions (Snell, Weisgerber, Helliwell, Weckert, Holzer, and Schroer, 1995). Reciprocal space mapping could well produce the necessary feedback in crystal quality to improve the growth control.

A two-dimensional reciprocal space map of a reflection from a 0.5-mm-diameter sample of lysozyme is given in Figure 14. The profile is exceedingly sharp (~5.5″ arc on the ω′ scale) indicative of a constant interplanar spacings for these length scales. The larger width parallel to the diffraction plane is indicative of some mosaicity that could also be observed by topography from this same reflection with a film close to the sample (position 1, Figure 6) (Fewster, Andrew, Snell,

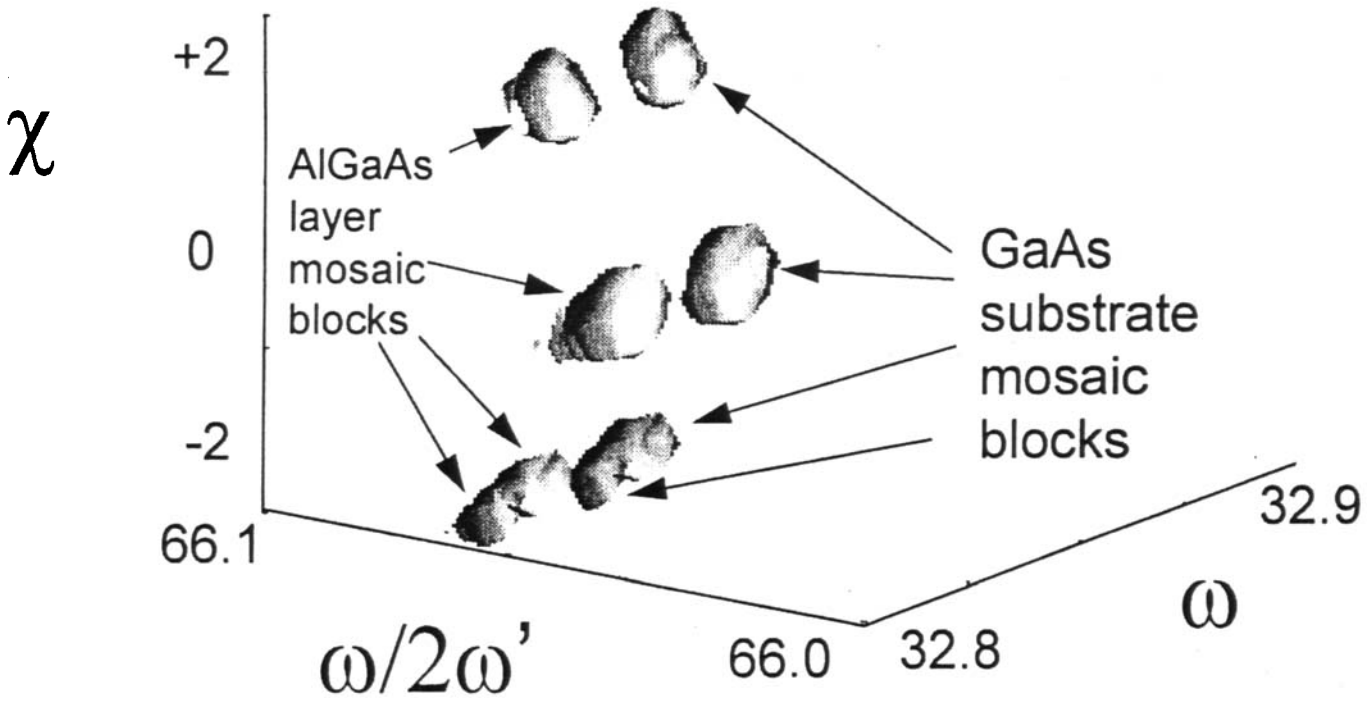

FIGURE 12. The three-dimensional reciprocal space map of the same sample as that of Figure 11. The mosaic blocks are now clearly separated and so their relative tilts and lattice parameters can be determined.

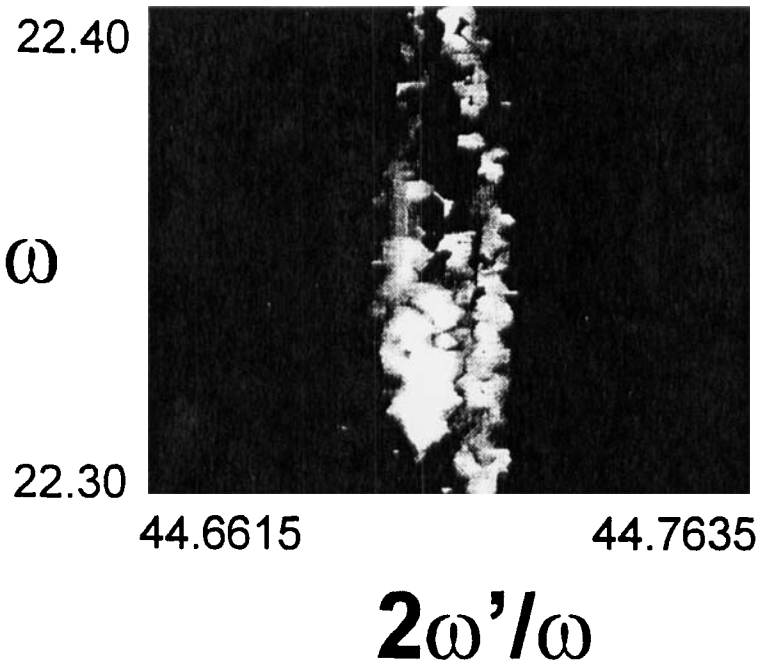

FIGURE 13. A three-dimensional reciprocal space map of the 002 reflection from a textured Al polycrystalline sample. Note the two main branches and the distribution of relative tilts and lattice parameters; from this it was possible to conclude that individual crystallites have slightly different lattice parameters.

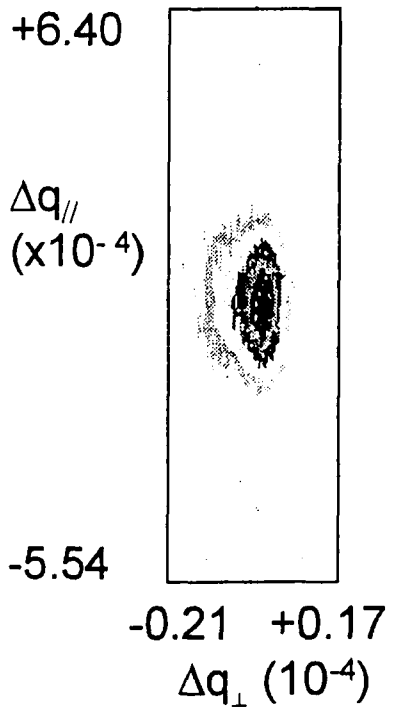

FIGURE 14. A reciprocal space map obtained from a biological macromolecule approximately 0.5 mm in diameter with a 2-kW X-ray source. These materials are extremely weakly scattering and can produce very sharp diffraction profiles (this profile has a full-width-at-half-maximum of 5.5″ arc on the ω′ scale).

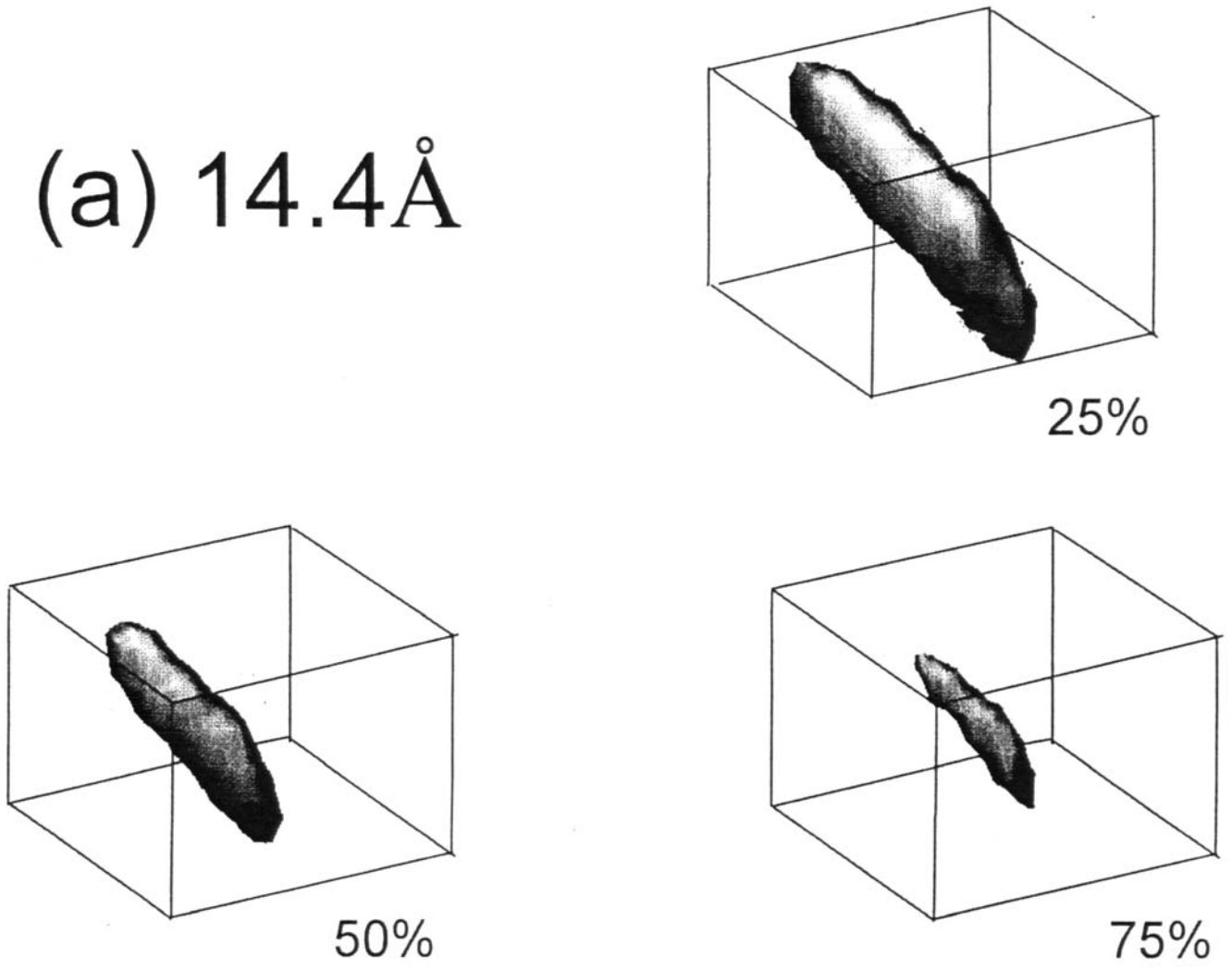

a

FIGURE 15. Three-dimensional reciprocal space maps of a lysozyme crystal taken at two different scattering angles that relate to length scales of 14.5 and 3Å. The dimensions from these shapes, when combined, will produce a deeper understanding of the structural nature of this crystal.

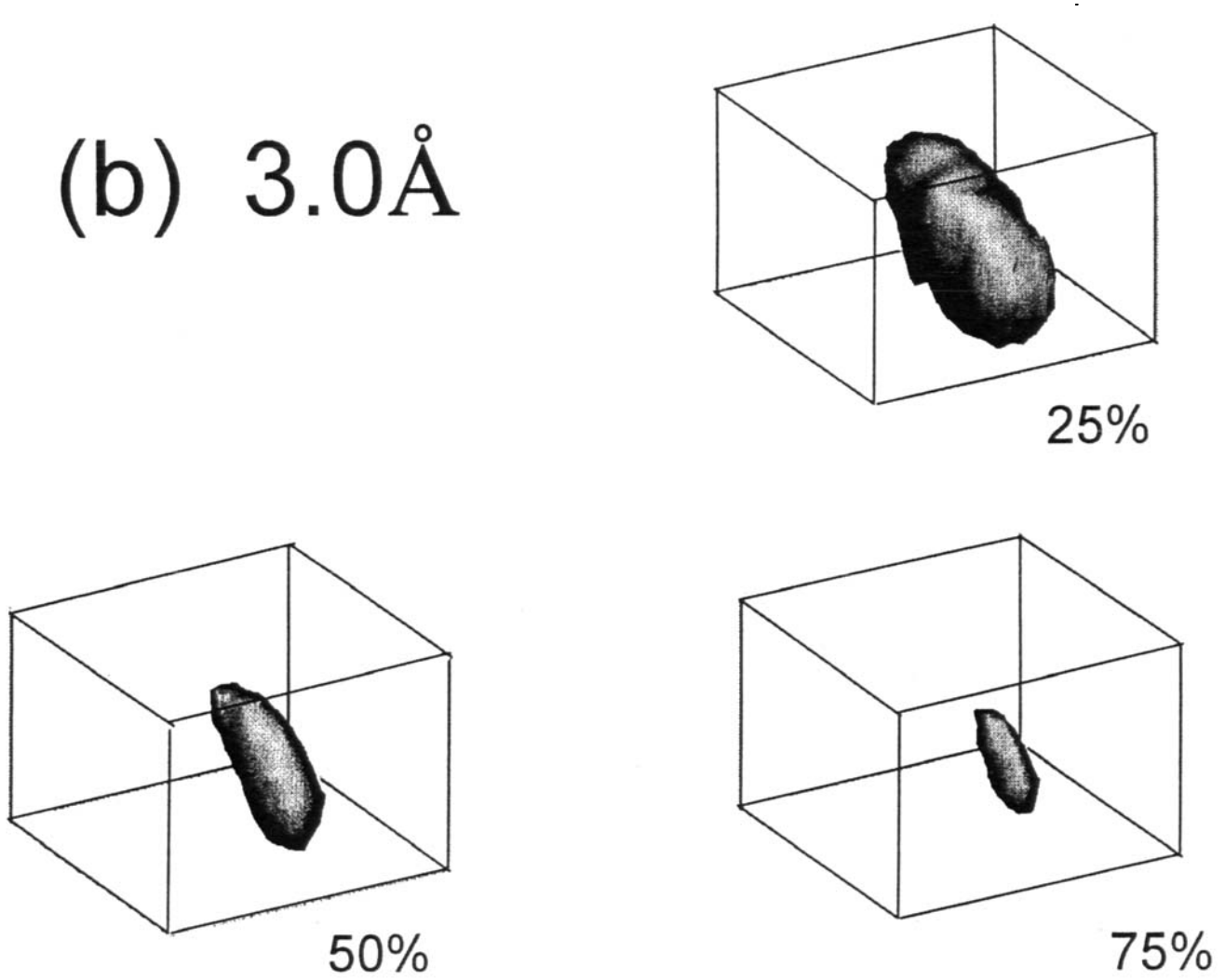

FIGURE 15b

Boggon, and Helliwell, 1996). The three-dimensional reciprocal space maps reveals more information and by combining the several reflections quantitative information can be obtained at various spatial resolutions (Figure 15).

VI. SUMMARY AND FUTURE

Reciprocal space mapping has now become well established as a powerful X-ray diffraction analysis method. The reason for this is the development of the multiple-crystal multiple-reflection diffractometer giving a wide range of analysis problems to be tackled on one instrument with only the sample alignment to consider. Of course, the instruments are available commercially and are all fully computer controlled. The range of settings can also be varied very easily so that the diffractometer can be set to solve the problem instead of the former situation when the problem was fitted to the diffractometer! Hence, changing from slit-based, low-resolution reciprocal space mapping to high-resolution, crystal-based reciprocal space mapping is now a rather straightforward exercise.

Reciprocal space mapping allows access to a considerable amount of data, which, as can be seen from this review, permits much more detailed information to be obtained. The analytical procedures will develop to fill the gap between the measured and predicted, or for that matter to explain unexpected features that appear in the reciprocal space maps. This will then lead to additional information about the structural details of materials. The finer details of most reciprocal space maps are rarely completely described. In high-resolution mode, the present day instrumentation will show deviations from perfection, even in some of the most "perfect" samples. For this reason the limit of the techniques is difficult to see. There is more information in a reciprocal space map than can presently be simulated; consequently, the method has a long future.

The range of applicability is clearly broadening, some of which has been alluded to in this review, for example, studies on semiconductors, ferroelectrics, polycrystalline materials, metallic multilayers, and even large biological macromolecules. In all these cases the single profile has been inadequate to obtain the information of interest. Of course, once the analysis has been performed with the most general methods, that is, reciprocal space mapping, such that a better understanding of the structural features are understood then a faster or a short-cut approach may be valid, because the assumptions are more clearly understood. Similarly reciprocal space mapping can prove very valuable in confirming the analysis from a short-cut approach, where there is an incomplete agreement with what might be expected from theoretical considerations.

ACKNOWLEDGMENT

I would like to thank Dr. Angeline Rehfeldt and Dr. Christopher Marshall for critically reading the manuscript.

REFERENCES

Barnett, S. J., Tanner, B. K., and Brown, G. T. *J. Mater. Res. Soc. Symp. Proc.* **41:** 83 (1985).

Birch, J., Sundgren, J-E., and Fewster, P. F. *J. Appl. Phys.* **78:** 6562 (1995).

Birch, J., Hjörvarsson, B., and Sundgren, J-E. private communication (1994).

Bond, W. L. *Acta Cryst.* **13:** 814 (1960).

Bonse, U. and Hart, M. *Appl. Phys. Lett.* **7:** 238 (1965).

Chu, S. N. G., Macrander, A. T., Strege, K. E., and Johnston, W. D. *J. Appl. Phys.* **57:** 249 (1985).

Coast-Smith, L. Ph.D. Thesis, University of Surrey (1997).

Coast-Smith, L., Kidd, P., and Fewster, P. F. unpublished work (1996).

Compton, A. H. *Phys. Rev.* **10:** 95 (1917).

Cowley, R. A. *Acta Cryst.* **A43:** 825 (1987).

Darhuber, A. A., Koppensteiner, E., Bauer, G., Wang, P. D., Song, Y. P., Sotomayor-Torres, C. M., and Holland, M. C. *J. Phys. D: Appl. Phys.* **28:** A195 (1995).

de Boer, D. K. G., Leenaers, A. J. G., and Wolf, R. M. *J. Phys. D: Appl. Phys.* **28:** A227 (1995).

Dederichs, P. H. *Phys. Rev.* **B4:** 1041 (1971).

Eaglesham, D. J., Kvam, E. P., Mayer, D. M., Humphreys, C. J., Green, G. S., Tanner, B. K., and Bean, J. C. *Appl. Phys. Lett.* **53:** 2083 (1988).

Fewster, P. F. *J. Appl. Cryst.* **18:** 334 (1985).

Fewster, P. F. *J. Appl. Cryst.* **22:** 64 (1989).

Fewster, P. F. *J. Appl. Cryst.* **24:** 178 (1991a).

Fewster, P. F. *Appl. Surf. Sci.* **50:** 9 (1991b).

Fewster, P. F. *J. Appl. Cryst.* **25:** 714 (1992).

Fewster, P. F. *J. Phys. D: Appl. Phys.* **26:** A142 (1993).

Fewster, P. F. *Appl. Phys.* **A58:** 121 (1994).

Fewster, P. F. *Rep. Progr. Phys.* **59:** 1339 (1996a).

Fewster, P. F. Reciprocal space mapping, in *X-Ray and Neutron Dynamical Diffraction: Theory and Applications*, Authier, A., Lagomarsino S., and Tanner, B. K., Eds., NATO ASI Series B: Physics **357,** Plenum Press, New York, 1996b, 269.

Fewster, P. F. and Andrew, N. L. Diffraction from thin layers, in *Materials Science Forum* **133,** Delhez, R. and Mittemeijer, E. J., Eds., *Trans Tech*, Switzerland, 1993a, 221.

Fewster, P. F. and Andrew, N. L. *J. Appl. Cryst.* **26:** 812 (1993b).

Fewster, P. F. and Andrew, N. L. *J. Appl. Phys.* **74:** 3121 (1993c).

Fewster, P. F. and Andrew, N. L. *J. Phys. D: Appl. Phys.* **28:** A97 (1995a).

Fewster, P. F. and Andrew, N. L. *J. Appl. Cryst.* **28:** 451 (1995b).

Fewster, P. F. and Andrew, N. L. Reciprocal space mapping and ultra-high-resolution diffraction from polycrystalline materials, in *Microstructure Analysis from Diffraction*, Oxford University Press, in press, 1996a.

Fewster, P. F. and Andrew, N. L. IUCr XVII Congress Seattle August 8 to 17, 1996, Symposium on Materials III: Strain and Stress Measurements, 1996b.

Fewster, P. F., Andrew, N. L., Snell, E. H., Boggon, T., and Helliwell, J. R. unpublished work (1996).

Fewster, P. F. and Curling, C. J. *J. Appl. Phys.* **62:** 4154 (1987).

Gailhanou, M., Baumbach, T., Marti, U., Silva, P. C., Reinhart, F. K., and Ilegems, M. *Appl. Phys. Lett.* **62:** 1623 (1993).

Gay, P., Hirsch, P. B., and Kelly, A. *Acta Metall.* **1:** 315 (1953).

Goorsky, M. S., Meshkinpour, M, Streit, D. C., and Block, T. R. *J Phys. D: Appl. Phys.* **28:** A92 (1995).

Hart, L. and Fewster, P. F. *Inst. Phys. Conf. Ser.* **134:** 569 (1993).

Hart, L., Fewster, P. F., Ashwin, M. J., and Newman, R. C., *J. Phys. D: Appl. Phys.* **28:** A154 (1995).

Heinke, H., Einfeld, S., Kuhn-Heinrich, B., Pahl, G., Möller, M. O., and Landwehr, G. *J. Phys. D: Appl. Phys.* **28** A104 (1995).

Heinke, H. and Möller, M. O., Hommel D., and Landwehr, G. *J. Cryst. Growth* **135:** 41 (1994).

Helliwell, J. R. *J. Cryst. Growth* **90:** 259 (1988).

Holý, V. *Appl. Phys.* **A58:** 173 (1994).

Holý, V. Dynamical theory of highly asymmetric X-ray diffraction, in *X-Ray and Neutron Dynamical Diffraction: Theory and Applications*, Authier, A., Lagomarsino, S., and Tanner, B. K., Eds., NATO ASI Series B: Physics **357,** Plenum Press, New York, 1996, 33.

Holý, V., Li, J. H., Bauer, G., Schäffler, F., and Herzog, H-J. *J. Appl. Phys.* **78:** 5013 (1995).

Holý, V. and Baumbach, T. *Phys. Rev.* **B49:** 10668 (1994).

Holý, V., Baumbach, T., and Bressière, M. *J. Phys. D: Appl. Phys.* **28:** A220 (1995).

Hu, Z. W. and Thomas P. A. IUCr XVII Congress Seattle August 8 to 17, 1996, Symposium on Microstructure and Texture, 1996.

Hu, Z. W., Thomas, P. A., and Webjörn, J. *J. Phys. D: Appl. Phys.* **28:** A189 (1995) .

Huang, K. *Proc. R. Soc.* **A190:** 102 (1947).

Iida, A. and Kohra, K. *Phys. Status Solidi* **A51:** 533 (1979).

Itoh. N. and Okamoto, K. *J. Appl. Phys.* **63:** 1486 (1988).

Jäger, W., Stenkamp, D., Ehrhardt, P., Leifer, K., Sybertz, W., Kibbel, H., Presting, H., and Kasper, E. *Thin Solid Films* **222:** 221 (1992).

Jordan-Sweet, J. L., Mooney, P. M., Lutz, M. A., Feenstra, R. M., Chu, J. O., and LeGroues, F. K. *J. Appl. Phys.* **80:** 89 (1996).

Kaganer, V. M., Köhler, R., Schmidbauer, M., Opitz, R. and Jenichen, B. submitted to *Phys. Rev. B* (1996).

Kato, N. *Acta Cryst.* **A36:** 763 (1980).

Kidd, P. and Fewster, P. F. *Mater. Res. Soc. Symp.* Proc. 317: 291 (1994).

Kidd, P., Fewster, P. F., and Andrew, N. L. *J. Phys. D: Appl. Phys.* **28:** A133 (1995).

Kidd, P., Fewster, P. F., Andrew, N. L., and Dunstan, D. J. *Inst. Phys. Conf. Ser. No.* **134:** Sect. 9, 585 (1993).

Koppensteiner, E., Ryan, T. W., Heuken, M., and Söllner, J. *J. Phys. D: Appl. Phys.* **26:** A35 (1993).

Koppensteiner, E., Hamberger, P., Bauer, G., Holý, V., and Kasper, E. *Appl. Phys. Lett.* **64:** 172 (1994).

Koppensteiner, E., Schuh, A., Bauer, G., Holý, V., Watson, G. P., and Fitzgerald, E. A. *J. Phys. D: Appl. Phys.* **28:** A114 (1995).

Krivoglaz, M. A. *Theory of X-ray Scattering by Real Crystals*, Plenum Press, New York, 1969.

Kyutt, R. N., Ruvimov, S. S., and Argunova, T. S. *J. Appl. Cryst.* **28:** 700 (1995).

Marra, W. C., Eisenberger, P., and Cho, A. Y. *J. Appl. Phys.* **50:** 6927 (1979).

Matyi, R. J., Melloch, M. R., Zhang, K., and Miller, D. L. *J. Phys. D: Appl. Phys.* **28:** A139 (1995).

Morilyansky, D. and Garstein, E. Third European Symposium on X-ray Topography and High Resolution Diffraction, Palermo, Italy, April 22 to 24, 1996.

Olsen, J. A., Hu, E. L., Lee, S. R., Fritz, I. J., Howard, A. J., Hammons, B. E., and Tsao, J. Y. *J. Appl. Phys.* **79:** 3578 (1996).

Peterson, I. R. and Kaganer, V. M. *Phys. Rev. Lett.* **73:** 102 (1994).

Picraux, S. T., Doyle, B. L. and Tsao, J. Y. Strain layer superlattices: material science and technology Pearsall, P., Ed., in *Semiconductor and Semimetals* Vol. 33, Academic Press, London, 1991, chap. 3.

Rossmanith, E. and Bengel, K. *Acta Cryst.* **A51:** 134 (1995).

Schectman, D., van Heerden, D., and Josell, D. *Mater. Lett.* **20:** 329 (1994).

Sinha, S. K., Sirota, E. B., Garoff, S., and Stanley, H. B. *Phys. Rev.* **B38:** 2297 (1988).

Snell, E. H., Weisgerber, S., Helliwell, J. R., Weckert, E., Holzer, K., and Schroer, K. *Acta Cryst.* **D52:** 529 (1995).

Stepanov, S. A., Kondrashkina, E. A., Schmidbauer, M., Köhler, R., Pfeiffer, J-U., Jach, T., and Suvirov, A. Yu. *Phys. Rev.* **B54:** 8150 (1996).

Stömmer, R., Grenzer, J., Fischer, J. and Pietsch, U. *J. Phys. D: Appl. Phys.* **28:** A216 (1995).

Tapfer, L., Sciacovelli, P. and De Caro, L. *J. Phys. D: Appl. Phys.* **28:** A179 (1995).

Thomas, J. E., Baldwin, T. O., and Dederichs, P. H. *Phys. Rev.* **B3:** 1167 (1971).

Thomson, L. R., Collins, G. J., Doyle, B. L., and Knapp, J. A. *J. Appl. Phys.* **70:** 4760 (1991).

Van der Sluis, P. *J. Phys. D: Appl. Phys.* **26:** A188 (1993).

van der Sluis, P. *Appl. Phys.* **A58:** 129 (1994).

van der Sluis, P., Binsma, J. J. M., and van Dongen, T. *Appl. Phys. Lett.* **62:** 3186 (1993).

Wang, V. S, Matyi, R. J., and Nordheden, K. J. *J. Appl. Phys.* **75:** 3835 (1994).

Warren, B. E. and Averbach, B. L. *J. Appl. Phys.* **21:** 595 (1950).

Williamson, G. K. and Hall, W. M. *Acta Metall.* **1:** 22 (1953).

Zaumseil, P. and Winter, U. *Phys. Status Solidi* **A70:** 497 (1982).

Zhang, X., Pashley, D. W., Hart, L., Neave, J. H., Fawcett, P. N., and Joyce, B. A. *J. Cryst. Growth* **143:** 300 (1993).